

# From Astrophysicist to Data Scientist in Three Acts: navigating an academic career with a short attention span

Jill P. Naiman  
Teaching Assistant Professor, iSchool  
[astronaiman.com](http://astronaiman.com)

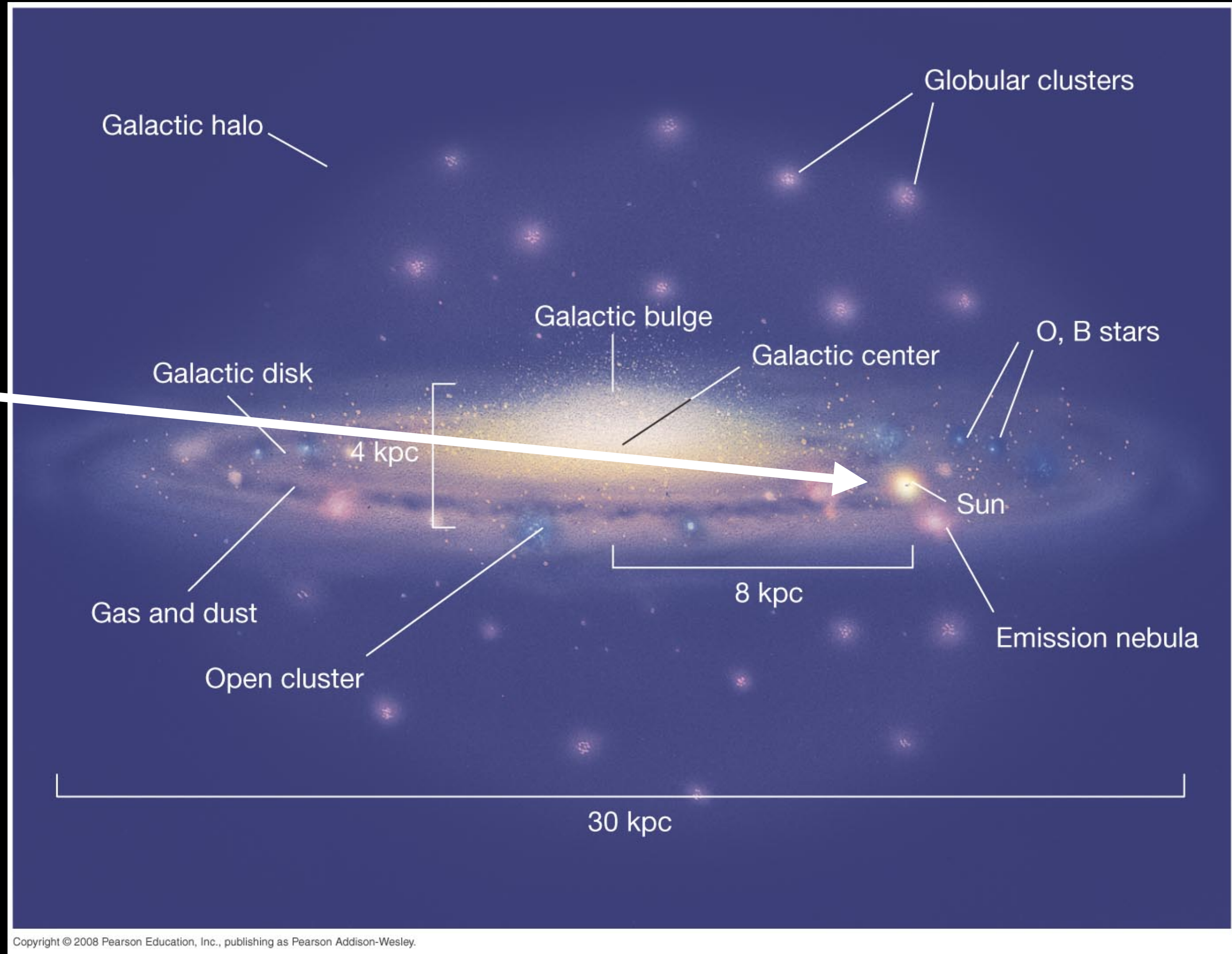
**Act I: Astronomy & Astrophysics**

**Act II: Data Visualization**

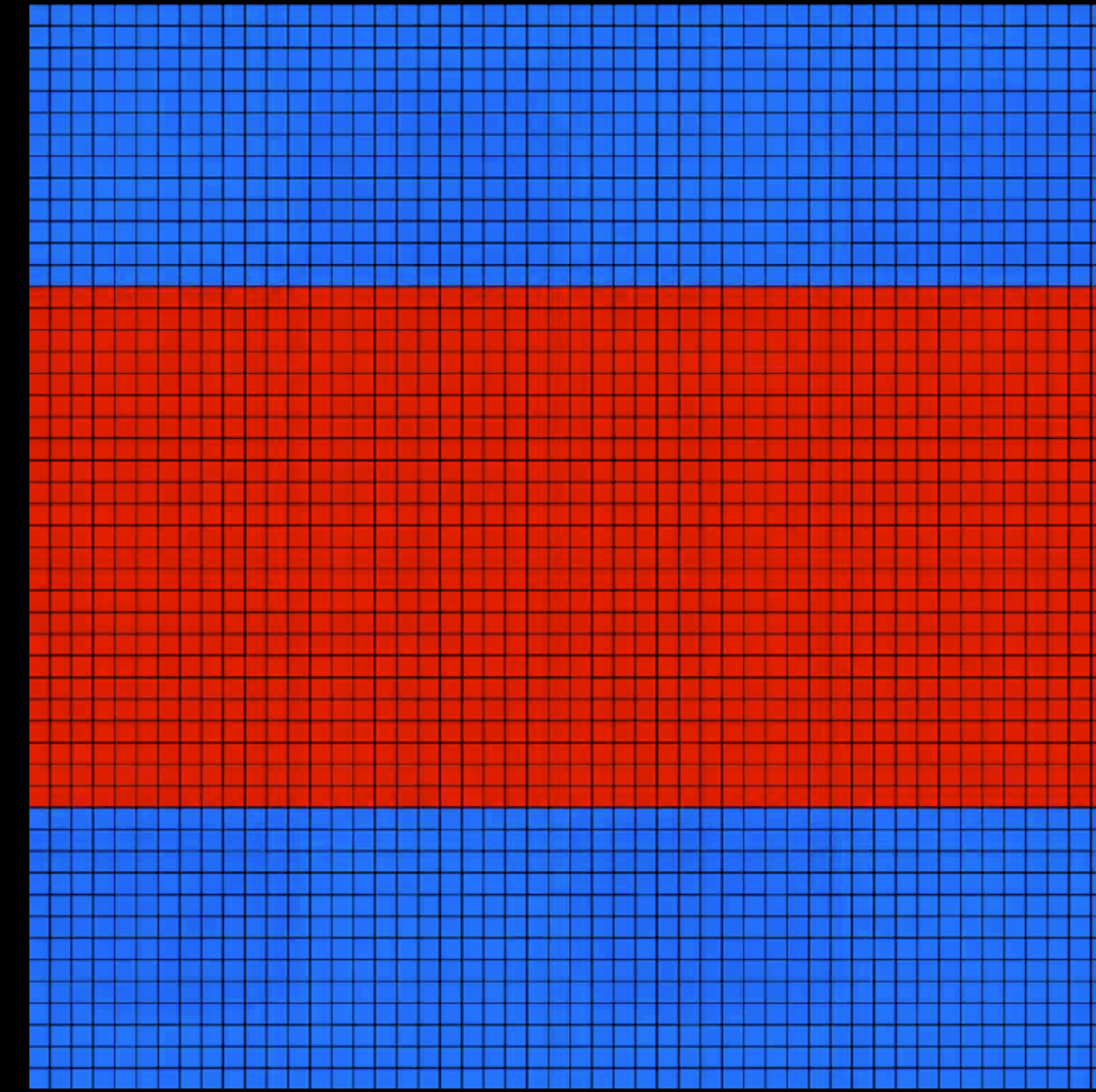
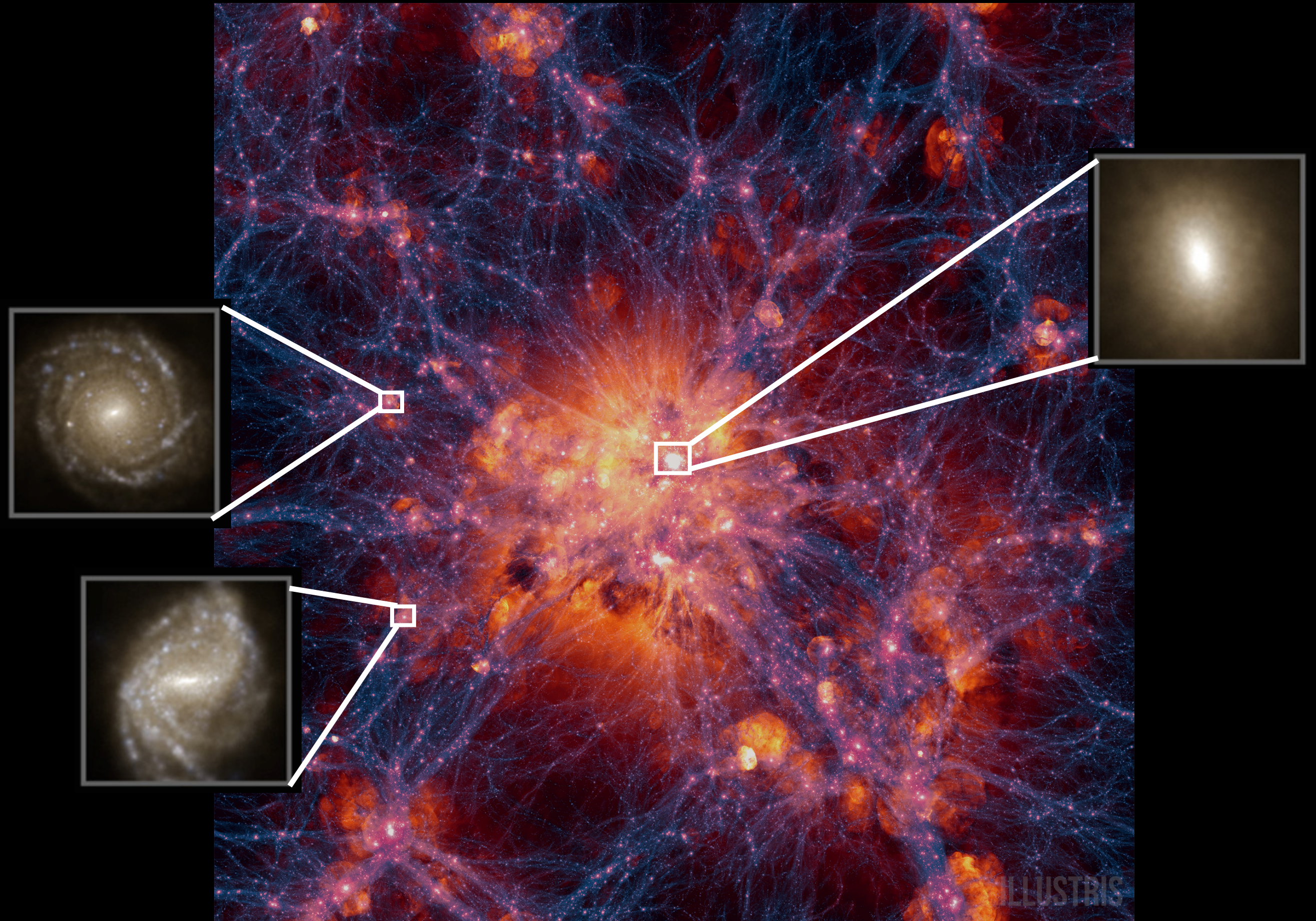
**Act III: Information Scientist?**

# **Act I: Astronomy & Astrophysics**

Earth is ~ here



# IllustrisTNG Simulations

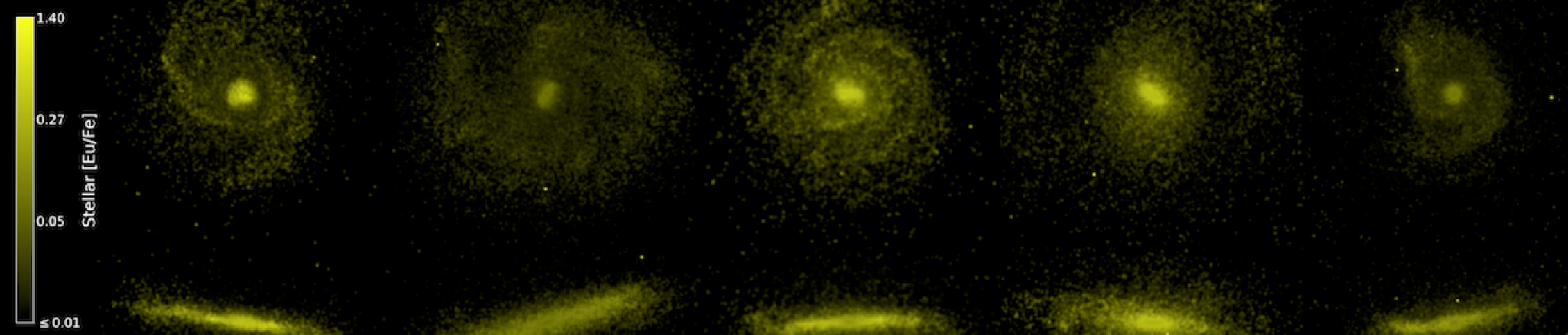
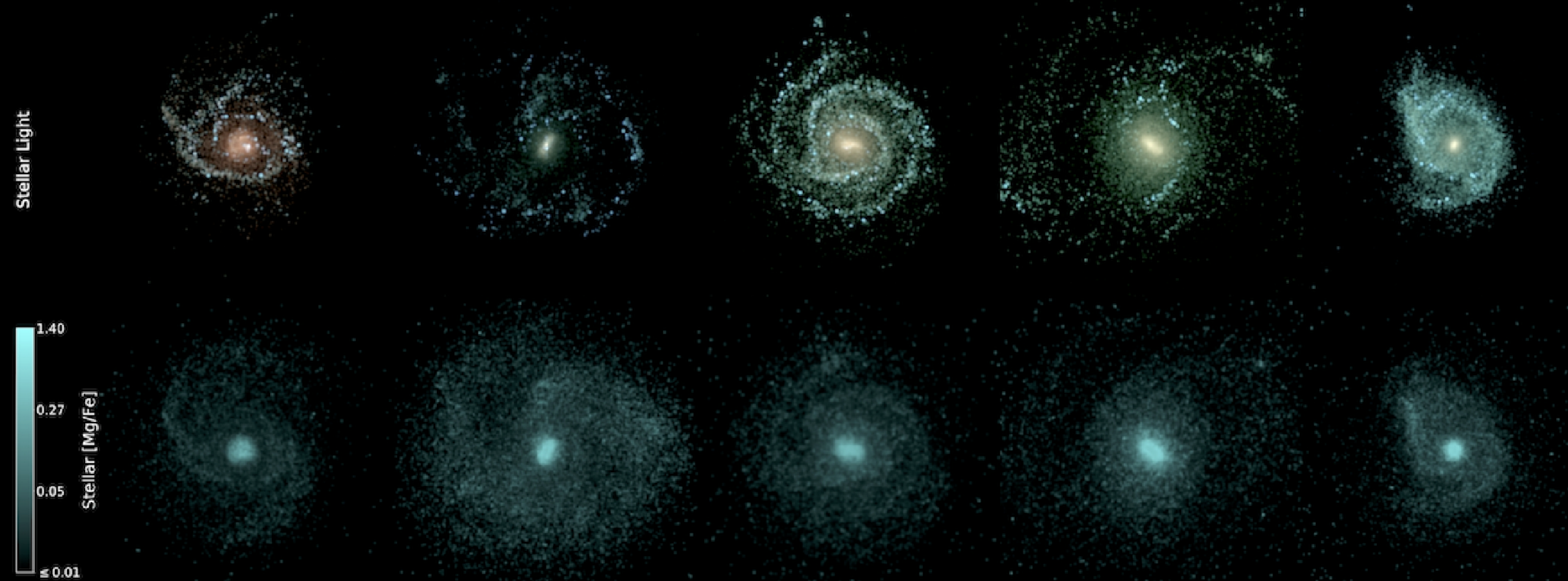


Moving mesh (AREPO)

# Simulating Cosmological Galaxy Formation: A Problem of Scales

1 Mpc  $\sim 3.1 \times 10^{22}$  meters

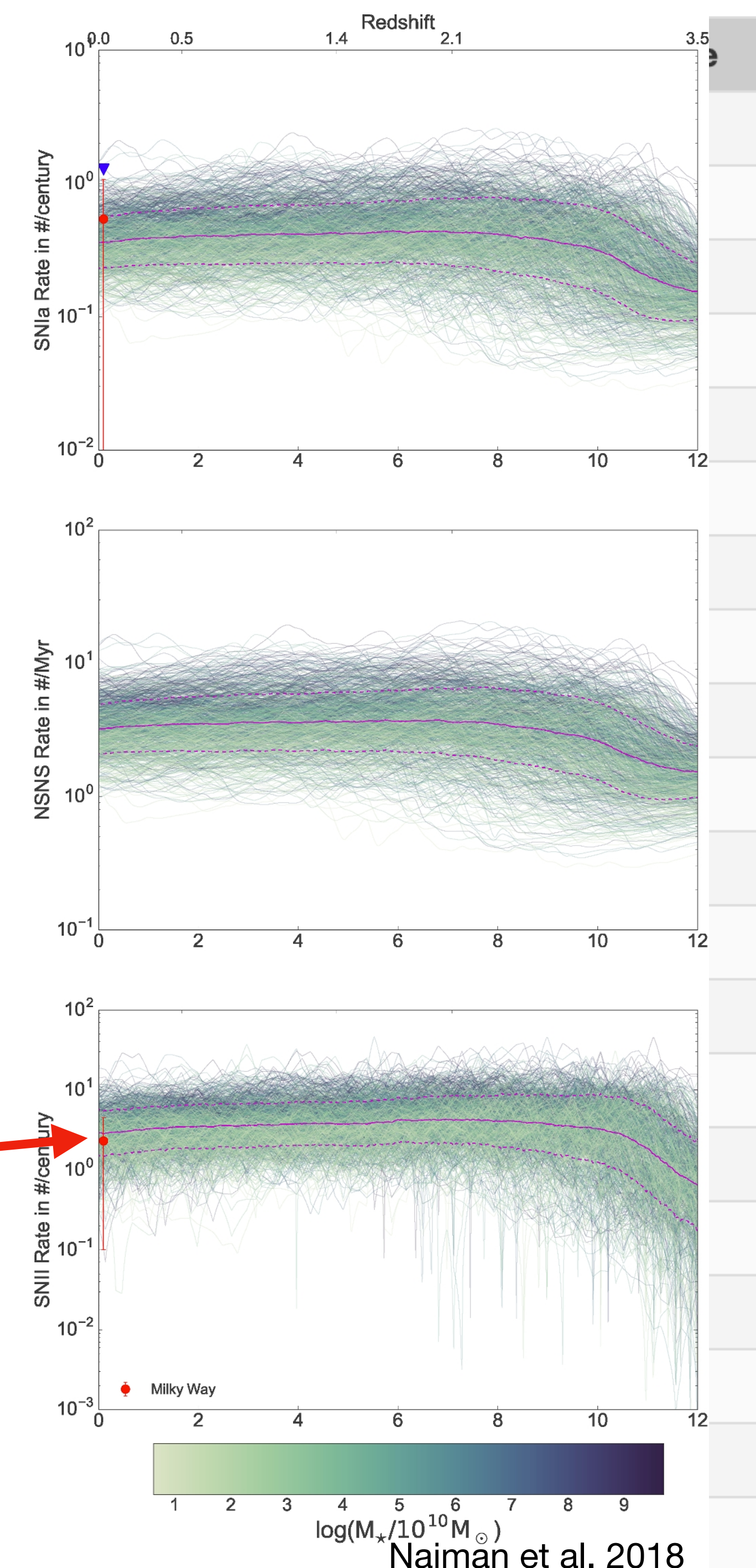
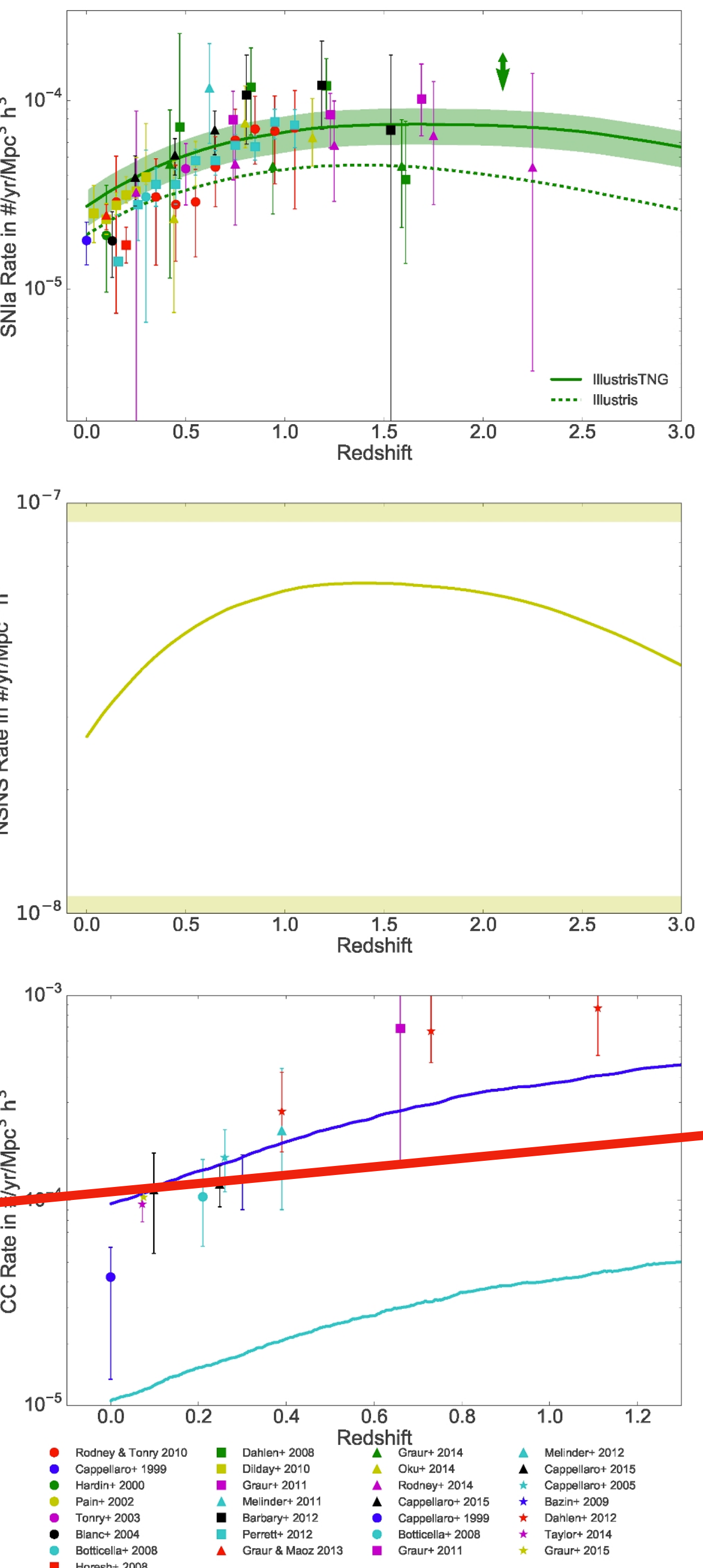
Credit: Nelson 2015



| Run             | Alt. Name     | Total NumPart (DM) | Chunks per Snapshot | Full Snapshot Size | Avg Groupcat Size | Total Data Volume |
|-----------------|---------------|--------------------|---------------------|--------------------|-------------------|-------------------|
| L35n270TNG      | TNG50-4       | 19,683,000         | 11                  | 5.2 GB             | 20 MB             | 0.6 TB            |
| L35n270TNG_DM   | TNG50-4-Dark  | 19,683,000         | 4                   | 1.2 GB             | 10 MB             | 0.1 TB            |
| L35n540TNG      | TNG50-3       | 157,464,000        | 11                  | 44 GB              | 130 MB            | 7.5 TB            |
| L35n540TNG_DM   | TNG50-3-Dark  | 157,464,000        | 4                   | 9.4 GB             | 50 MB             | 0.6 TB            |
| L35n1080TNG     | TNG50-2       | 1,259,712,000      | 128                 | 350 GB             | 860 MB            | 18 TB             |
| L35n1080TNG_DM  | TNG50-2-Dark  | 1,259,712,000      | 85                  | 76 GB              | 350 MB            | 4.5 TB            |
| L35n2160TNG     | TNG50-1       | 10,077,696,000     | 680                 | 2.7 TB             | 7.2 GB            | ~320 TB           |
| L35n2160TNG_DM  | TNG50-1-Dark  | 10,077,696,000     | 128                 | 600 GB             | 2.3 GB            | 36 TB             |
| L75n455TNG      | TNG100-3      | 94,196,375         | 7                   | 27 GB              | 110 MB            | 1.5 TB            |
| L75n455TNG_DM   | TNG100-3-Dark | 94,196,375         | 4                   | 5.7 GB             | 40 MB             | 0.4 TB            |
| L75n910TNG      | TNG100-2      | 753,571,000        | 56                  | 215 GB             | 650 MB            | 14 TB             |
| L75n910TNG_DM   | TNG100-2-Dark | 753,571,000        | 8                   | 45 GB              | 260 MB            | 2.8 TB            |
| L75n1820TNG     | TNG100-1      | 6,028,568,000      | 448                 | 1.7 TB             | 4.3 GB            | 128 TB            |
| L75n1820TNG_DM  | TNG100-1-Dark | 6,028,568,000      | 64                  | 360 GB             | 1.7 GB            | 22 TB             |
| L205n625TNG     | TNG300-3      | 244,140,625        | 16                  | 63 GB              | 340 MB            | 4 TB              |
| L205n625TNG_DM  | TNG300-3-Dark | 244,140,625        | 4                   | 15 GB              | 130 MB            | 1 TB              |
| L205n1250TNG    | TNG300-2      | 1,953,125,000      | 100                 | 512 GB             | 2.2 GB            | 31 TB             |
| L205n1250TNG_DM | TNG300-2-Dark | 1,953,125,000      | 25                  | 117 GB             | 810 MB            | 7.2 TB            |
| L205n2500TNG    | TNG300-1      | 15,625,000,000     | 600                 | 4.1 TB             | 14 GB             | 235 TB            |
| L205n2500TNG_DM | TNG300-1-Dark | 15,625,000,000     | 75                  | 930 GB             | 5.2 GB            | 57 TB             |

| Run             | Alt. Name     | Total NumPart (DM) | Chunks per Snapshot | Full Snapshot Size | Avg Groupcat Size | Total Data Volume |
|-----------------|---------------|--------------------|---------------------|--------------------|-------------------|-------------------|
| L35n270TNG      | TNG50-4       | 19,683,000         | 11                  | 5.2 GB             | 20 MB             | 0.6 TB            |
| L35n270TNG_DM   | TNG50-4-Dark  | 19,683,000         | 4                   | 1.2 GB             | 10 MB             | 0.1 TB            |
| L35n540TNG      | TNG50-3       | 157,464,000        | 11                  | 44 GB              | 130 MB            | 7.5 TB            |
| L35n540TNG_DM   | TNG50-3-Dark  | 157,464,000        | 4                   | 9.4 GB             | 50 MB             | 0.6 TB            |
| L35n1080TNG     | TNG50-2       | 1,259,712,000      | 128                 | 350 GB             | 860 MB            | 18 TB             |
| L35n1080TNG_DM  | TNG50-2-Dark  | 1,259,712,000      | 85                  | 76 GB              | 350 MB            | 4.5 TB            |
| L35n2160TNG     | TNG50-1       | 10,077,696,000     | 680                 | 2.7 TB             | 7.2 GB            | ~320 TB           |
| L35n2160TNG_DM  | TNG50-1-Dark  | 10,077,696,000     | 128                 | 600 GB             | 2.3 GB            | 36 TB             |
| L75n455TNG      | TNG100-3      | 94,196,375         | 7                   | 27 GB              | 110 MB            | 1.5 TB            |
| L75n455TNG_DM   | TNG100-3-Dark | 94,196,375         | 4                   | 5.7 GB             | 40 MB             | 0.4 TB            |
| L75n910TNG      | TNG100-2      | 753,571,000        | 56                  | 215 GB             | 650 MB            | 14 TB             |
| L75n910TNG_DM   | TNG100-2-Dark | 753,571,000        | 8                   | 45 GB              | 260 MB            | 2.8 TB            |
| L75n1820TNG     | TNG100-1      | 6,028,568,000      | 448                 | 1.7 TB             | 4.3 GB            | 128 TB            |
| L75n1820TNG_DM  | TNG100-1-Dark | 6,028,568,000      | 64                  | 360 GB             | 1.7 GB            | 22 TB             |
| L205n625TNG     | TNG300-3      | 244,140,625        | 16                  | 63 GB              | 340 MB            | 4 TB              |
| L205n625TNG_DM  | TNG300-3-Dark | 244,140,625        | 4                   | 15 GB              | 130 MB            | 1 TB              |
| L205n1250TNG    | TNG300-2      | 1,953,125,000      | 100                 | 512 GB             | 2.2 GB            | 31 TB             |
| L205n1250TNG_DM | TNG300-2-Dark | 1,953,125,000      | 25                  | 117 GB             | 810 MB            | 7.2 TB            |
| L205n2500TNG    | TNG300-1      | 15,625,000,000     | 600                 | 4.1 TB             | 14 GB             | 235 TB            |
| L205n2500TNG_DM | TNG300-1-Dark | 15,625,000,000     | 75                  | 930 GB             | 5.2 GB            | 57 TB             |

| Run             | Alt. Name     | Total NumPart (DM) | Chun  |
|-----------------|---------------|--------------------|---|
| L35n270TNG      | TNG50-4       | 19,683,000         |   |
| L35n270TNG_DM   | TNG50-4-Dark  | 19,683,000         |   |
| L35n540TNG      | TNG50-3       | 157,464,000        |   |
| L35n540TNG_DM   | TNG50-3-Dark  | 157,464,000        |   |
| L35n1080TNG     | TNG50-2       | 1,259,712,000      |   |
| L35n1080TNG_DM  | TNG50-2-Dark  | 1,259,712,000      |   |
| L35n2160TNG     | TNG50-1-Dark  | 10,077,696,000     | <ul style="list-style-type: none"> <li>• Data “chunking”</li> </ul>   |
| L75n455TNG      | TNG100-3      | 94,196,375         |   |
| L75n455TNG_DM   | TNG100-3-Dark | 94,196,375         | <ul style="list-style-type: none"> <li>• Python in parallel on supercomputers/multi-core computers (5-50 CPUs)</li> </ul> |
| L75n910TNG      | TNG100-2      | 753,571,000        |   |
| L75n910TNG_DM   | TNG100-2-Dark | 753,571,000        |   |
| L75n1820TNG     | TNG100-1      | 6,028,568,000      |   |
| L75n1820TNG_DM  | TNG100-1-Dark | 6,028,568,000      |   |
| L205n625TNG     | TNG300-3      | 244,140,625        | <ul style="list-style-type: none"> <li>Thousands of Milky Way-like (our galaxy) star formation histories</li> </ul>       |
| L205n625TNG_DM  | TNG300-3-Dark | 244,140,625        |   |
| L205n1250TNG    | TNG300-2      | 1,953,125,000      |   |
| L205n1250TNG_DM | TNG300-2-Dark | 1,953,125,000      |   |
| L205n2500TNG    | TNG300-1      | 15,625,000,000     |   |
| L205n2500TNG_DM | TNG300-1-Dark | 15,625,000,000     | tng-project.com   |

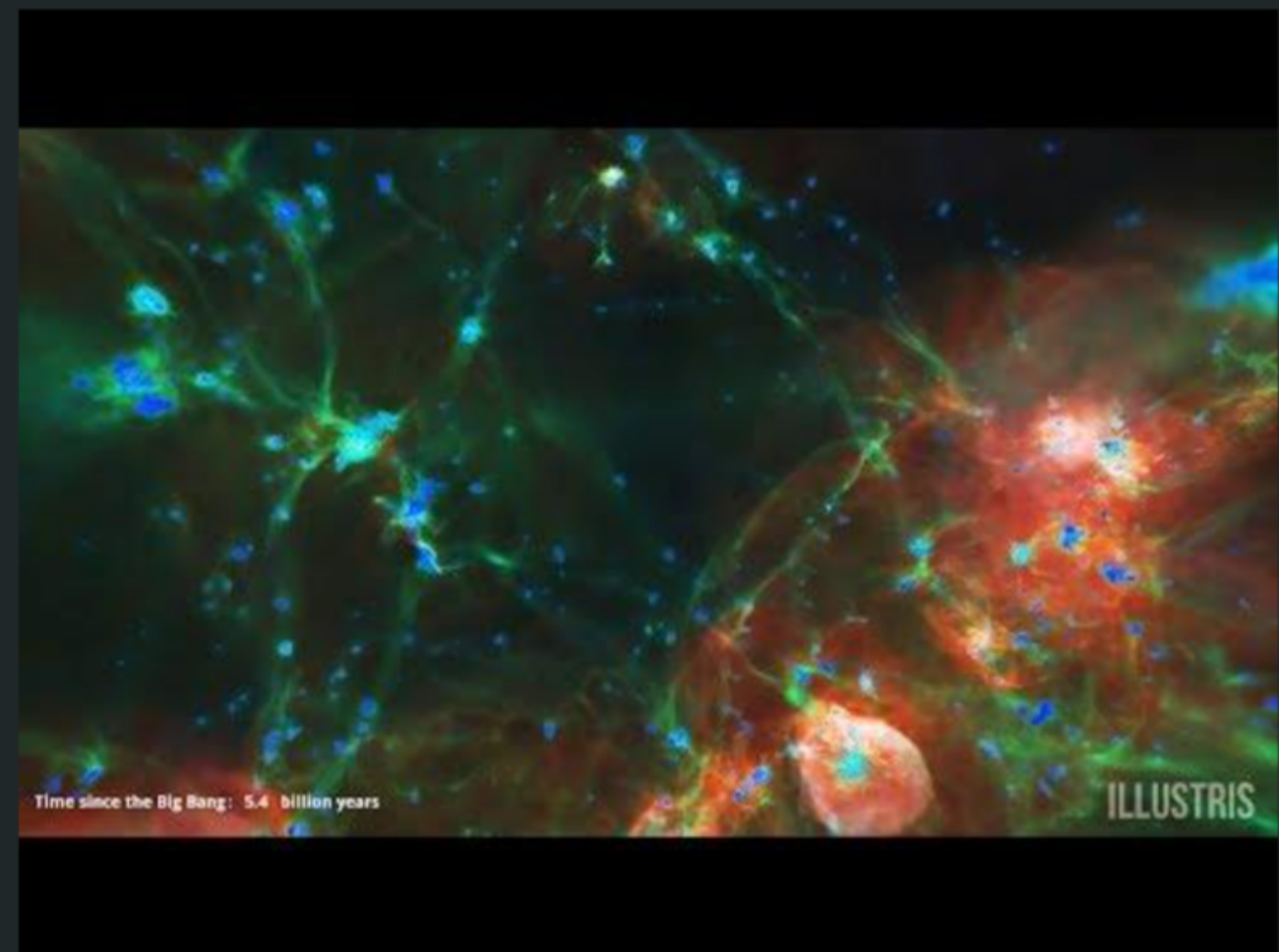


Naiman et al. 2018

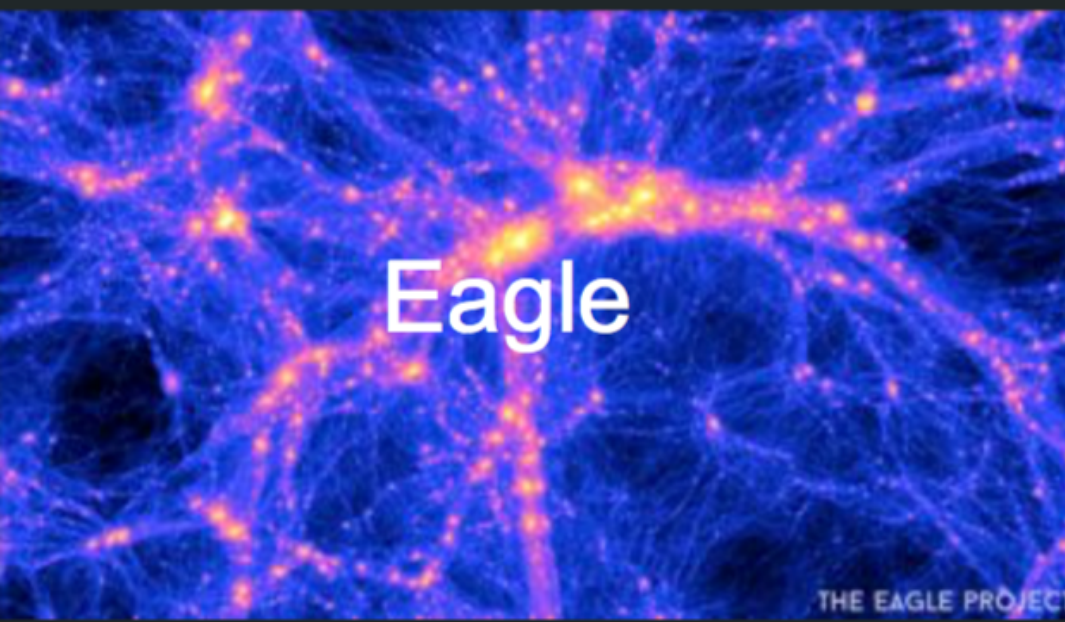
- Rodney & Tonry 2010
- Cappellaro+ 1999
- Hardin+ 2000
- Dilday+ 2010
- Graur+ 2011
- Melinder+ 2011
- Barbary+ 2012
- Perrett+ 2012
- Botticella+ 2008
- Graur & Maoz 2013
- Graur+ 2011
- Graur+ 2014
- Cappellaro+ 2015
- Bazin+ 2009
- Dahlen+ 2012
- Taylor+ 2014
- Graur+ 2015
- Melinder+ 2012
- Cappellaro+ 2005
- Cappellaro+ 1999
- Cappellaro+ 2008
- Dahlen+ 2014
- Dilday+ 2014
- Graur+ 2014
- Melinder+ 2011
- Cappellaro+ 2015
- Bazin+ 2009
- Dahlen+ 2012
- Taylor+ 2014
- Graur+ 2015
- Melinder+ 2012
- Cappellaro+ 2015
- Cappellaro+ 2005
- Cappellaro+ 1999
- Cappellaro+ 2008
- Dahlen+ 2014
- Dilday+ 2014
- Graur+ 2014
- Melinder+ 2011
- Cappellaro+ 2015
- Bazin+ 2009
- Dahlen+ 2012
- Taylor+ 2014
- Graur+ 2015

# Act II: Data Visualization

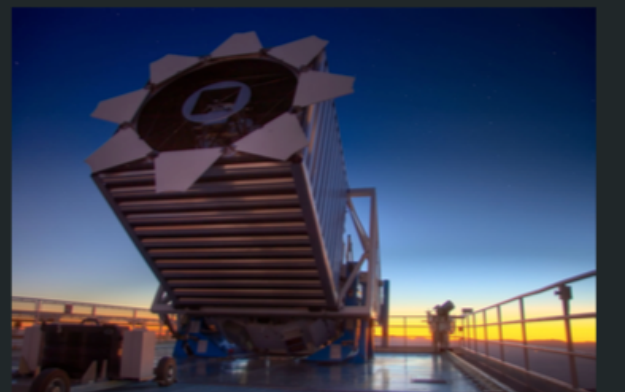
# Scientists have lots of data



IllustrisTNG: Tens of TB



## Scientists have lots of data



Sloan Digital Sky Survey: ~ 120TB (already)



Dark Energy Survey: ~200GB/night, ~PB last decade

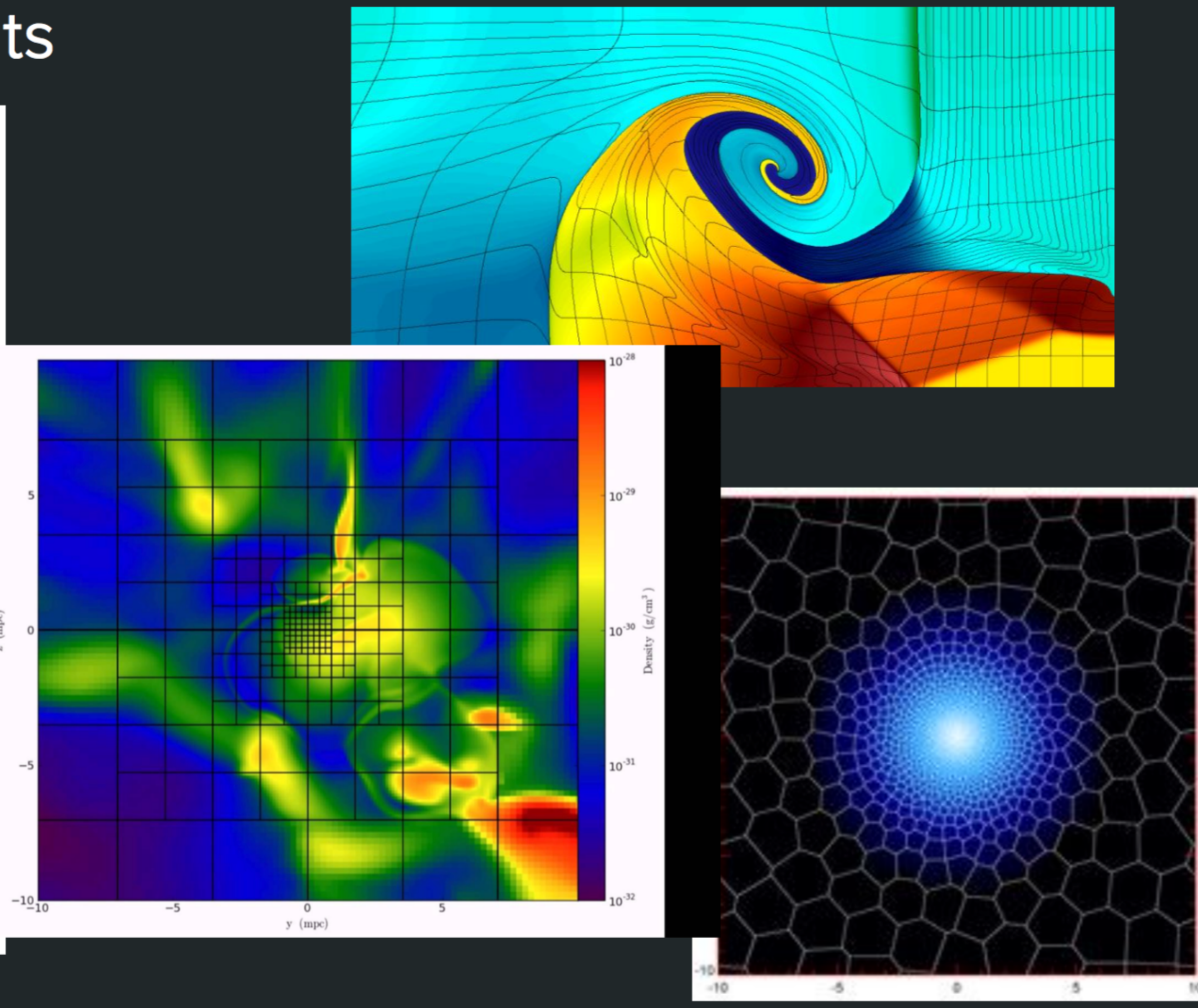
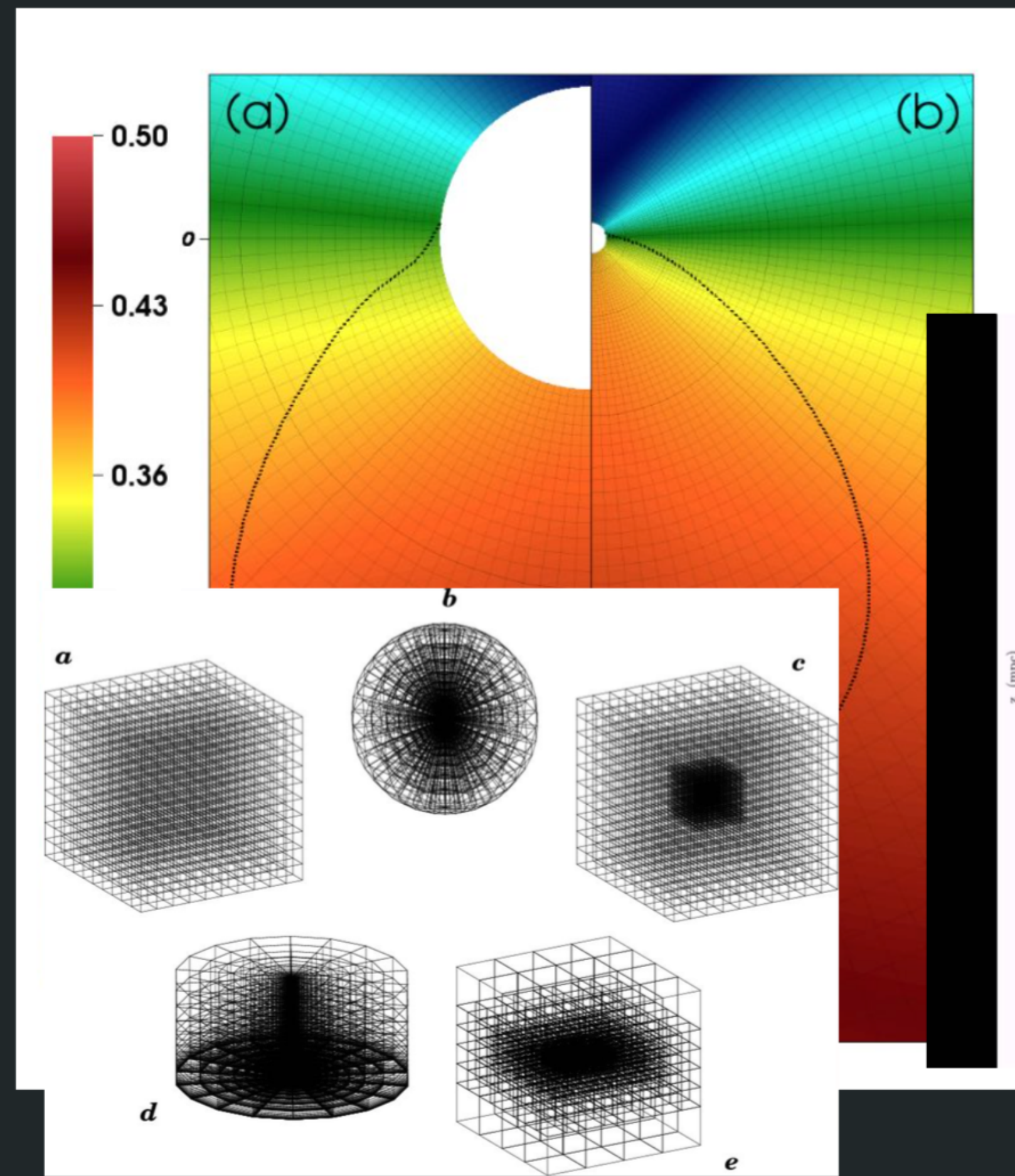


Large Synoptic Survey Telescope - 200PB/decade



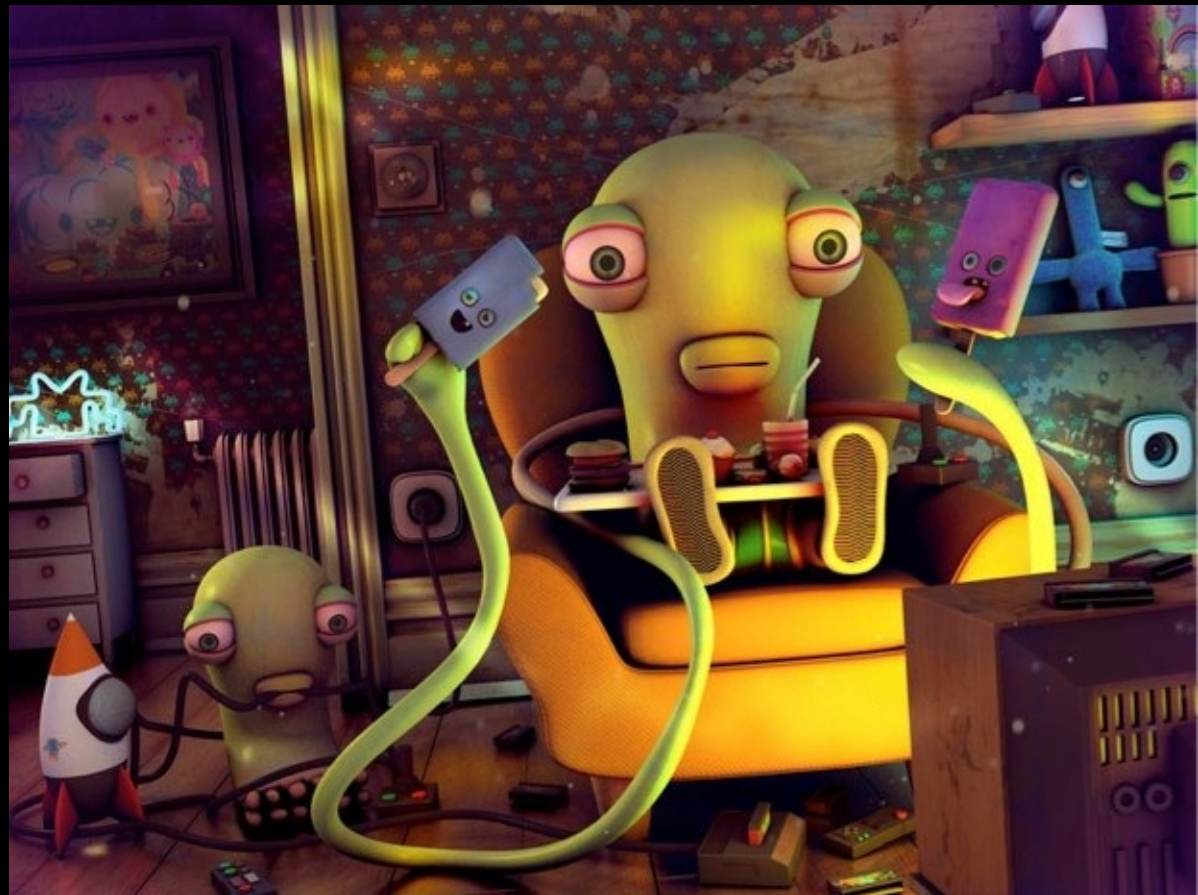
Square Kilometre Array: 1000PB/year

# The Data is in weird formats



# Blender

- 3D modeling and animating program (free Maya)
- used by 3D graphics folks and a few astronomers
- Python API

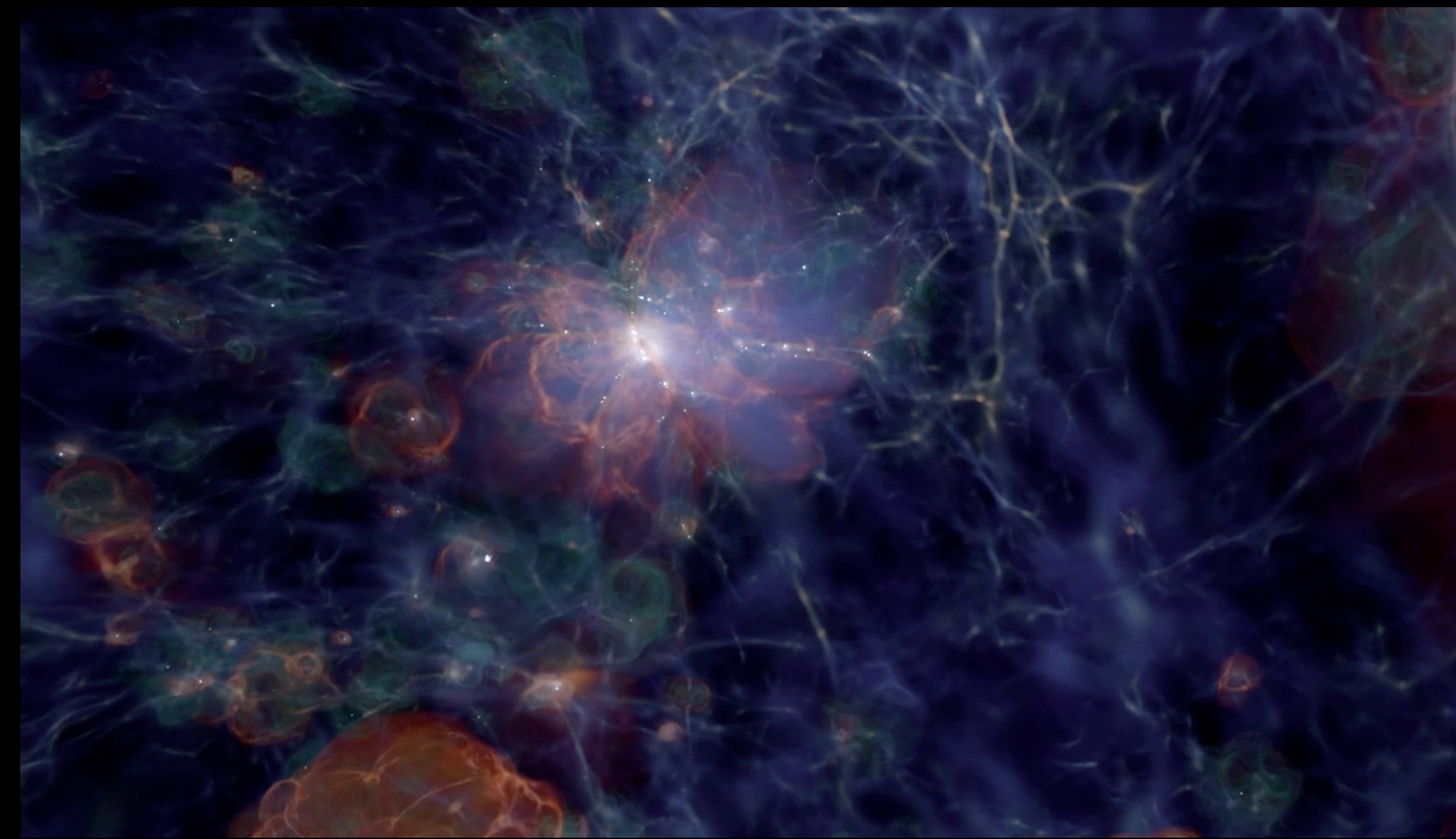


Gab 2012 <http://gablich.wordpress.com/>

# Houdini™



Visualization with the Advanced Visualization Lab (NCSA)



[http://www.ncsa.illinois.edu/enabling/vis/cadens/documentation/beginning\\_of\\_time](http://www.ncsa.illinois.edu/enabling/vis/cadens/documentation/beginning_of_time)

[ytini.com/blog.html](http://ytini.com/blog.html)



“Raw”



ytini



# Scientific Visualization as an Educational Tool

## Workshops/Short courses:

<https://www.astroblend.com/ba2016/>

<https://www.astroblend.com/ba2017/>

[https://jnaiman.github.io/csci-p-14110\\_su2020/](https://jnaiman.github.io/csci-p-14110_su2020/)

[https://jnaiman.github.io/csci-p-14110\\_su2019/](https://jnaiman.github.io/csci-p-14110_su2019/)

# Scientific Visualization as an Educational Tool

## Workshops/Short courses:

<https://www.astroblend.com/ba2016/>

<https://www.astroblend.com/ba2017/>

[https://jnaiman.github.io/csci-p-14110\\_su2020/](https://jnaiman.github.io/csci-p-14110_su2020/)

[https://jnaiman.github.io/csci-p-14110\\_su2019/](https://jnaiman.github.io/csci-p-14110_su2019/)

[https://uiuc-ischool-dataviz.github.io/is445\\_spring2022/](https://uiuc-ischool-dataviz.github.io/is445_spring2022/)

# Act III: Information Science?

(Digitization? Curriculum development? Visualization analytics? Science nomad?)

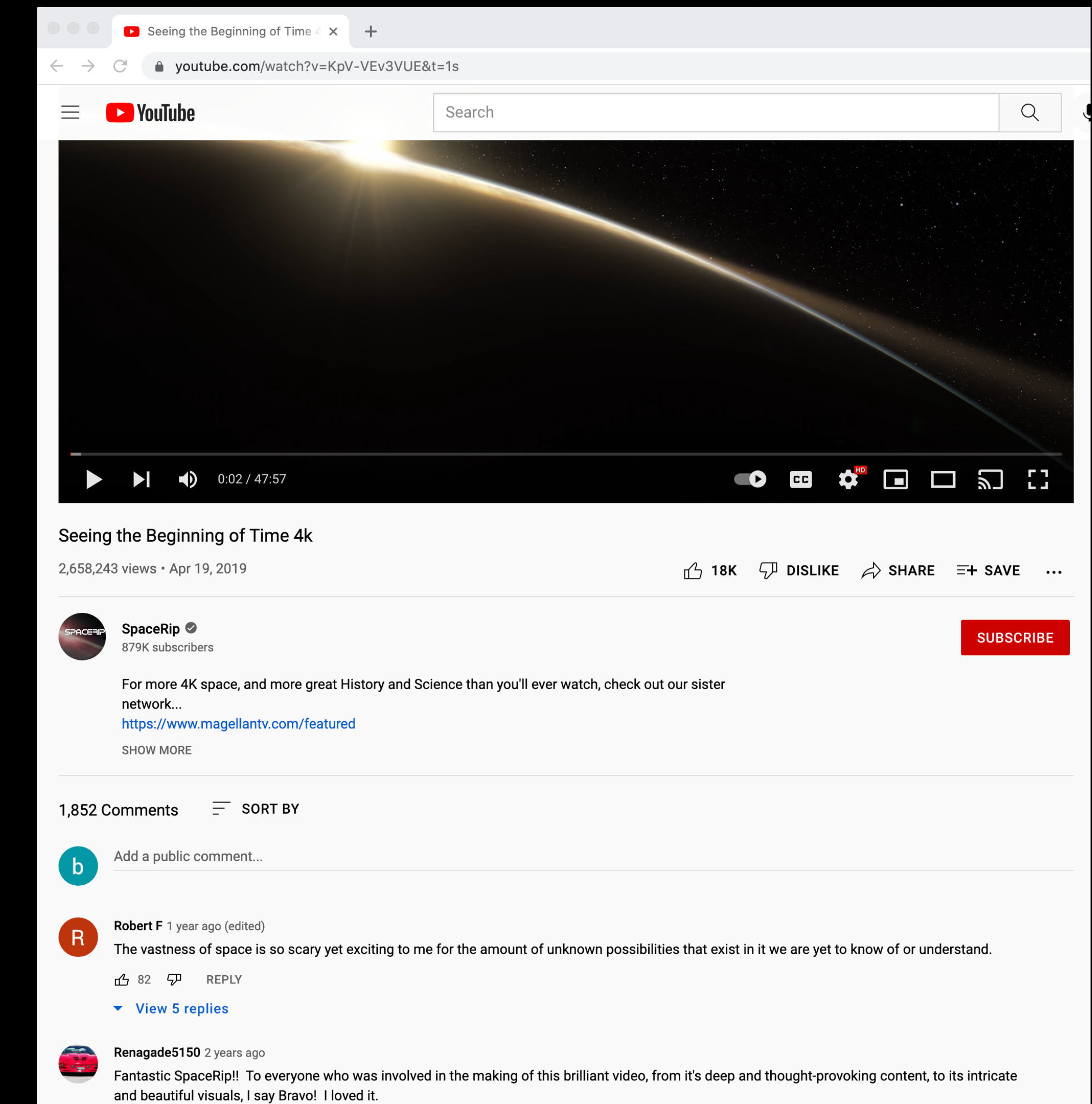
# Impact Analysis with NLP on AVL Documentaries

Based on Rezapour & Diesner 2017

With iSchool students: Alistair Nunn, Anuska Gami, Shriya Srikanth  
& in collaboration with the AVL

|   |   |
|---|---|
| Positive shift in <b>knowledge</b>        | “Very educational...learned a lot”  |
| Negative shift in <b>knowledge</b>        | “This is the biggest lie”   |
| Positive <b>interest</b> in science topic | “My heart warms as we uncover the most unique and fascinating secrets of the universe”      |
| Negative <b>interest</b> in science topic | “A waste of time and resources”   |
| Positive <b>engagement</b> with film      | “I like the piano”  |
| Negative <b>engagement</b> with film      | “Man this narrator gets pretty annoying after 7-10 min”                                     |
| Impersonal report                         | “From the intro, none of this exists yet”   |
| Personal opinion                          | “There will be a time when they all will be face to face with the creator of the universal” |

Table from Anushka Gami (Oct 11th SPIN talk)





Kalina Borkiewicz



Jeff Carpenter



Stuart Levy



Eric Jensen  
Brinson Civic Science Fellow  
Assoc. Prof. University of Warwick, Sociology



NCSA | National Center for  
Supercomputing Applications

AVL | Advanced Visualization Lab



School of Information Sciences



Jill Naiman

# Digitizing Science: Indexing the Astronomical Literature

1840 A. R. MARSTON: RINGS AROUND WR STARS

**Table** Multiple ring nebulae observed.

|      | Filter     | Exposure (secs) | Figure |
|------|------------|-----------------|--------|
| WR10 | H $\alpha$ | 1800            | 2      |
| WR40 | H $\alpha$ | 900             | 3a     |
| WR40 | [OIII]     | 2100            | 3b     |
| WR75 | H $\alpha$ | 1950            | 4a     |
| WR75 | [OIII]     | 2100            | 4b     |
| WR75 | H $\alpha$ | 2700            | 1a     |
| WR85 | [OIII]     | 2700            | 1b     |
| WR85 | H $\alpha$ | 900             | 5      |

\* uses the nomenclature of van der Hucht et al. (1981).

ejection events. This uses a similar line of argument to that proposed by Balick *et al.* (1992) for using the extended halos of planetary nebulae to distinguish the characteristics of the red giant stellar winds that existed prior to their formation.

In this paper, we provide new, deep imaging of a number of multiple rings observed around WR stars in an optical narrow-band survey made of WR stars in the southern skies. We discuss their possible implications for WR evolution and postulate what further information they may provide about the evolution of massive stars with closer investigation.

**2. OBSERVATIONS**

Narrow-band imaging, using H $\alpha$  ( $\lambda=6563 \text{ \AA}$ ,  $\Delta\lambda=12 \text{ \AA}$ ) and [O III] ( $\lambda=5006 \text{ \AA}$ ,  $\Delta\lambda=44 \text{ \AA}$ ) filters was performed using a Thomson 1024 $\times$ 1024 CCD chip at the  $f/3$  focus of the 0.6 m Curtis Schmidt at Cerro Tololo Interamerican Observatory (CTIO) during the nights of 15–19 May 1994. The sample objects were taken from the lists of Marston *et al.* (1994) and Marston & Yocom (in preparation). It was intended that all possible shells associated with the WR stars would be identified as well as information on relative sizes and morphologies. A full listing of observations used in this paper are supplied in Table 1.

**3. RESULTS ON MULTIPLE RINGS**

Images of the multiple ring systems of our sample are shown in Figs 1(a) and 1(b). These images allow us to study the bipolar shapes of the nebulae and apparent sizes of the multiple shells.

**Fig Caption**

Fig 1. (a) H $\alpha$  image of the filamentary, bipolar nebula RCW104 surrounding the WR star WR75. (b) Deep [O III] image of the wind-blown bubble at the center of RCW104.

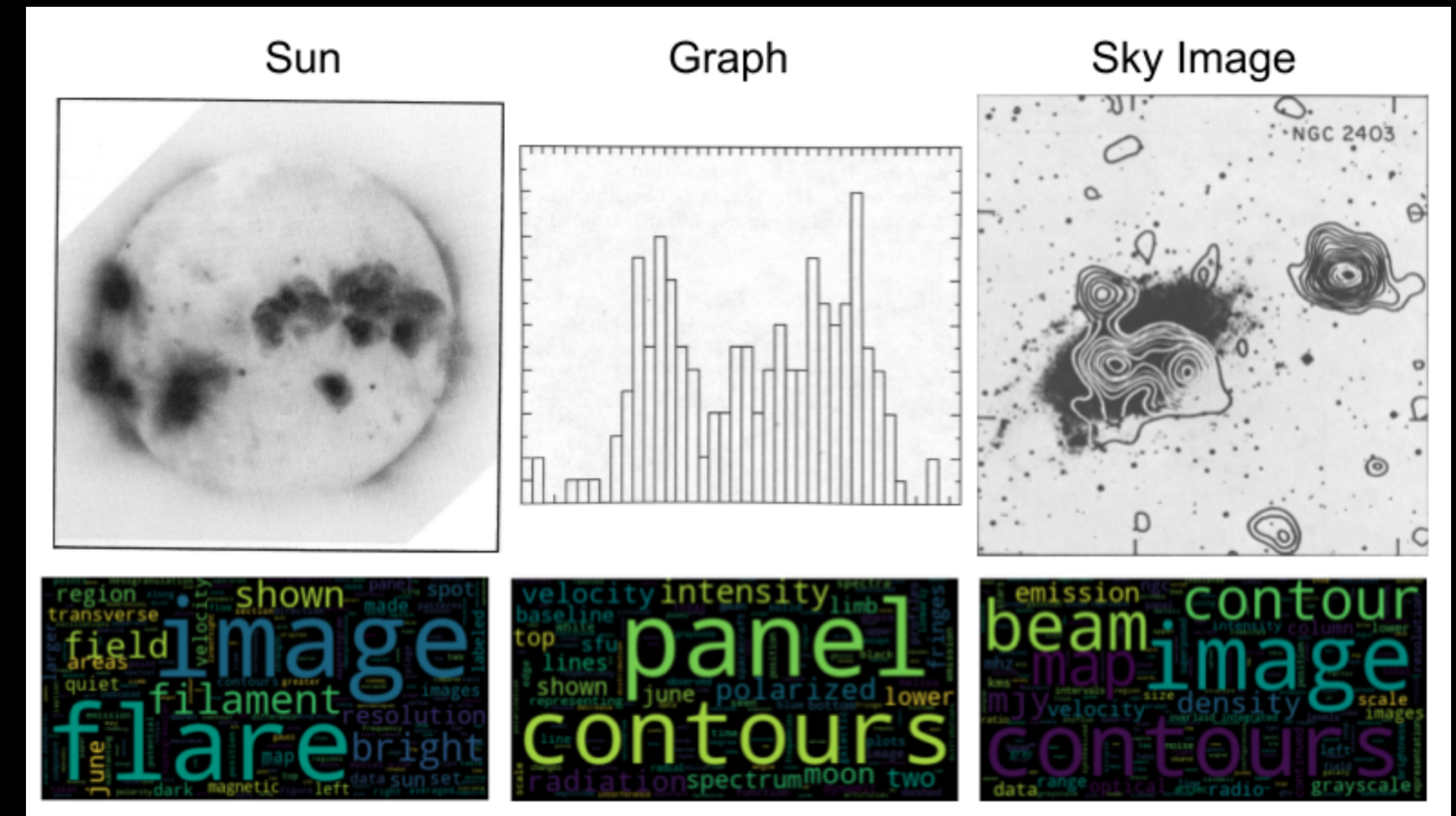
**3.1 Bipolar Shells**

Figures 1(a) and 1(b) show new, deep images of the nebula RCW 104 in both H $\alpha$  and [O III] which surrounds the WR star WR75. This is the only object in our sample to show a bipolar morphology in H $\alpha$ . However, close inspection of Fig. 1 of Marston *et al.* (1994) shows that the nebula NGC 2359 around the star WR6 has a diffuse outer, bipolar shell, which extends to approximately  $20'$  from the central star. The bright shell in the center is only  $5'$  across. NGC 2359 has been shown to have multiple velocity components which may be associated with multiple ejections (Goudis *et al.* 1994). Ejected material appears to be interacting with the diffuse bipolar materials as well as a nearby molecular cloud (Marston 1991; Schneps *et al.* 1981). The shell around

WR75 shows similar multiple components. An outer bipolar flow is outlined by strong H $\alpha$  filaments in the central regions while fainter lobes are observed to the north and south, extending to around  $15'$  from the central WN6 star. An inner ring of [O III] emitting material is observed entirely within the bipolar outflow and is only  $10'$  in diameter. The outer filaments of RCW 104 have been spectroscopically observed by Esteban *et al.* (1990), who suggest their abundances are similar to that expected from the enhanced abundances in a RSG wind. We might interpret our observation of these two bipolar nebulae as being the RSG ejecta outer filaments and relatively young WR winds interacting with the ejecta to form central cavities. The expansion of the cavities has not yet reached the edge of the RSG ejecta.

In both cases of bipolar morphology, a wind-blown (W)

© American Astronomical Society • Provided by the NASA Astrophysics Data System



Jill P. Naiman

+ Peter Williams & Alyssa Goodman (Harvard, Seamless Astronomy)

+ Ishita Ghosh, Toby Tao, Shantanu Pagare, Ayesha Baweja, Linh Pham (iSchool)

| TABLE 1. Multiple ring nebulae observed. |           |               |            |                 |        |
|--|-----------|---------------|------------|-----------------|--------|
| WR star*                                 | ID Number | Date observed | Filter     | Exposure (secs) | Figure |
| WR16                                     | HD86161   | 16 May 1994   | H $\alpha$ | 1800            | 2      |
| WR30                                     | HD94005   | 15 May 1994   | H $\alpha$ | 900             | 3a     |
| WR40                                     | HD96548   | 18 May 1994   | H $\alpha$ | 1950            | 3b     |
| WR40                                     |           | 19 May 1994   | [OIII]     | 2100            | 4b     |
| WR75                                     | HD14749   | 17 May 1994   | H $\alpha$ | 1700            | 1a     |
| WR75                                     | HD14749   | 17 May 1994   | [OIII]     | 2700            | 1b     |
| WR88                                     | HR6392B   | 16 May 1994   | H $\alpha$ | 900             | 5      |

\* uses the nomenclature of van der Hucht et al. (1988).

ejection events. This uses a similar line of argument to that proposed by Balick *et al.* (1992) for using the extended halos of planetary nebulae to distinguish the characteristics of the red giant stellar winds that existed prior to their formation.

In this paper, we provide new, deep imaging of a number of multiple rings observed around WR stars in an optical narrow-band survey made of WR stars in the southern skies. We discuss their possible implications for WR evolution and postulate what further information they may provide about the evolution of massive stars with closer investigation.

## 2. OBSERVATIONS

Narrow-band imaging, using H $\alpha$  ( $\lambda=6563$  Å,  $\Delta\lambda=12$  Å) and [O III] ( $\lambda=5007$  Å,  $\Delta\lambda=44$  Å) was performed using a Thermo 1024×1024 CCD chip at the f/3 focus of the 1.5 m Curtis Schmidt at Cerro Tololo Inter-American Observatory (CTIO) during the nights of 15–19 May 1994. The sample objects were taken from the lists of Marston *et al.* (1994) and Marston & Yocom (in preparation). It was intended that all possible shells associated with the WR stars would be identified as well as information on relative sizes and morphologies. A full listing of observations used in this paper are supplied in Table 1.

## 3. RESULTS ON MULTIPLE RINGS

Images of the multiple ring systems of our sample are shown in Figs. 1–5. These reveal nebulae whose morphologies allow a classification into two distinct types. Those with bipolar shapes in an outer ejecta shell, and those with more spherical outer shells. Table 2 lists the ring type (after Chu 1991) and apparent sizes of the multiple shells.

### 3.1 Bipolar Shells

WR75 shows similar multiple components. An outer bipolar flow is outlined by strong H $\alpha$  filaments in the central regions while fainter lobes are observed to the north and south, extending to around 15° from the central WN9 star. An inner ring of [O III] emitting material is observed entirely within the bipolar outflow and is only 10° in diameter. The outer filaments of RCW104 have been spectroscopically observed by Esteban *et al.* (1990), who suggest their abundances are similar to those expected from the enhanced abundances in a RSG wind. We might interpret our observations of these two bipolar nebulae as being RSG ejected outer filaments and relatively young WR winds interacting with the ejecta to form central cavities. The expansion of the cavities has not yet reached the edge of the RSG ejecta.

In both cases of bipolar morphology, a wind-blown (W)

© American Astronomical Society • Provided by the NASA Astrophysics Data System

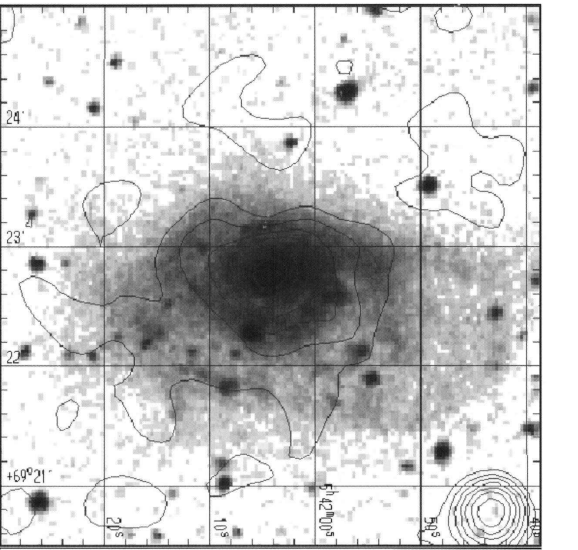


FIG. 1. The HRI data (contours) are overlaying the optical image of NGC 1961 from the digitized sky survey. The X-ray data have been smoothed with a Gaussian with  $\sigma=10''$  and the contour levels are  $(6.66, 7.77, 8.88, 9.98, 11.09, 12.20, 13.31, 14.42, 15.53, 16.64) \times 10^{-2}$  counts  $s^{-1}$  arcmin $^{-2}$ .

37'') centered on the peak of the emission from the northwest quadrant of the galaxy, we determine the count rate is  $5.58 \times 10^{-3} \pm 0.73 \times 10^{-3}$  counts  $s^{-1}$ , which corresponds to an X-ray luminosity of  $7.26 \times 10^{41}$  erg  $s^{-1}$ . The count rate from the nuclear region is  $2.58 \times 10^{-3} \pm 0.32 \times 10^{-3}$  counts  $s^{-1}$  which corresponds to an X-ray luminosity of  $3.2 \times 10^{41}$  erg  $s^{-1}$  in a 22'' circular aperture. This implies that the X-ray luminosity from the disk of this galaxy is at least  $7.9 \times 10^{41}$  erg  $s^{-1}$ .

## 3. OPTICAL DATA

Images in a variety of passbands and spectral data were acquired for both galaxies to trace both young and old stellar components. Narrow-band images, with filters (of typical bandwidth 60 Å) isolating H $\beta$ , [O III]  $\lambda\lambda 5007, \lambda\lambda 4959, \lambda\lambda 4971$ , and [S II]  $\lambda\lambda 6717, 6731$  at each galaxy's redshift, along with adjacent continuum bands at 5125 and 6694 Å for continuum subtraction, were obtained at the KPNO 2.1 m telescope with the video-camera system in 1984 October. The field of view was 140 arcsec, well matched to the size of NGC 2276 and requiring two pointings for NGC 1961 (so that only the central part was observed in the H $\beta$ , [O III], and [S II] passbands). Additional broad-band images were obtained with CCDs for NGC 2276 (in *B* at the KPNO 2.1 m and *BVRI* at the Lowell 1.1 m) and NGC 1961 (*BRI* and narrow band for H $\alpha$ ). The Video Camera data used a combination of internal quartz and night-sky flat fields, with geometric distortions produced by the image-tube chain corrected after flat-field division. Since it corrects to constant

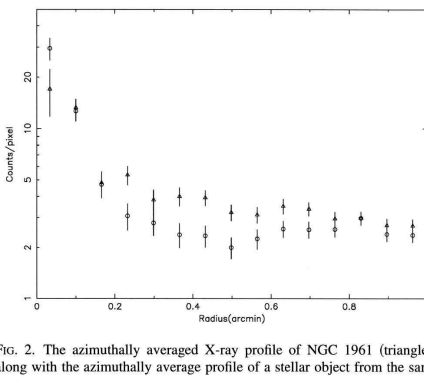


FIG. 2. The azimuthally averaged X-ray profile of NGC 1961 (triangles) along with the azimuthally average profile of a stellar object from the same image (crosses). NGC 1961 has excess emission from 0.25 to 0.75.

© American Astronomical Society • Provided by the NASA Astrophysics Data System

# The Dataset

## A. A. MICHELSON

to which it is subject in consequence of the attraction of the sun and moon and as modified by the resulting distortion of the body of the earth. But this may be furnished with any desired degree of accuracy by the changes in the position of the level of a liquid surface which is necessarily normal to the resultant of all the forces acting. If from these we can eliminate all but the gravitational forces the problem is solved.

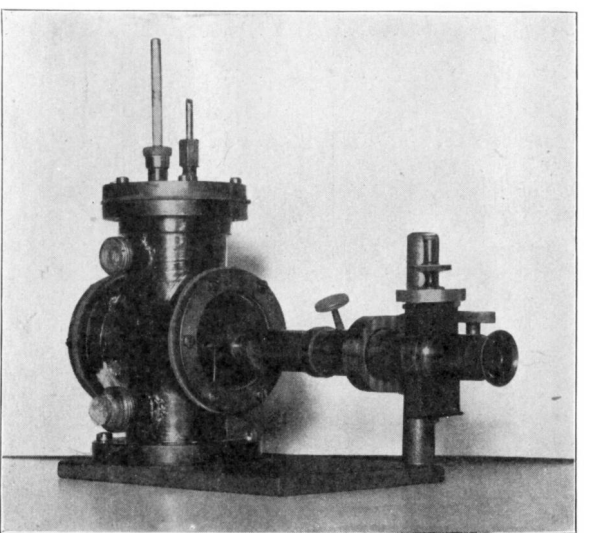


FIG. 1.—Microscope and gauge

A very sensitive method of measuring the changes in level is furnished by the interferometer; and a method of carrying this into practice was devised and the apparatus constructed\* in 1910.

But before attempting to utilize so delicate an appliance it was deemed advisable to make these preliminary experiments with the microscope. Accordingly a 6-inch pipe, 500 feet long, was half filled with water,\* the level of which could be read off through the glass sides of the end vessels, as shown in Fig. 1.

\* An interference apparatus for this purpose was independently devised by Professor A. G. Webster.

\* The vessels at the ends were at first connected by a pipe filled with water, but with this arrangement temperature changes produced enormous disturbances in the level.

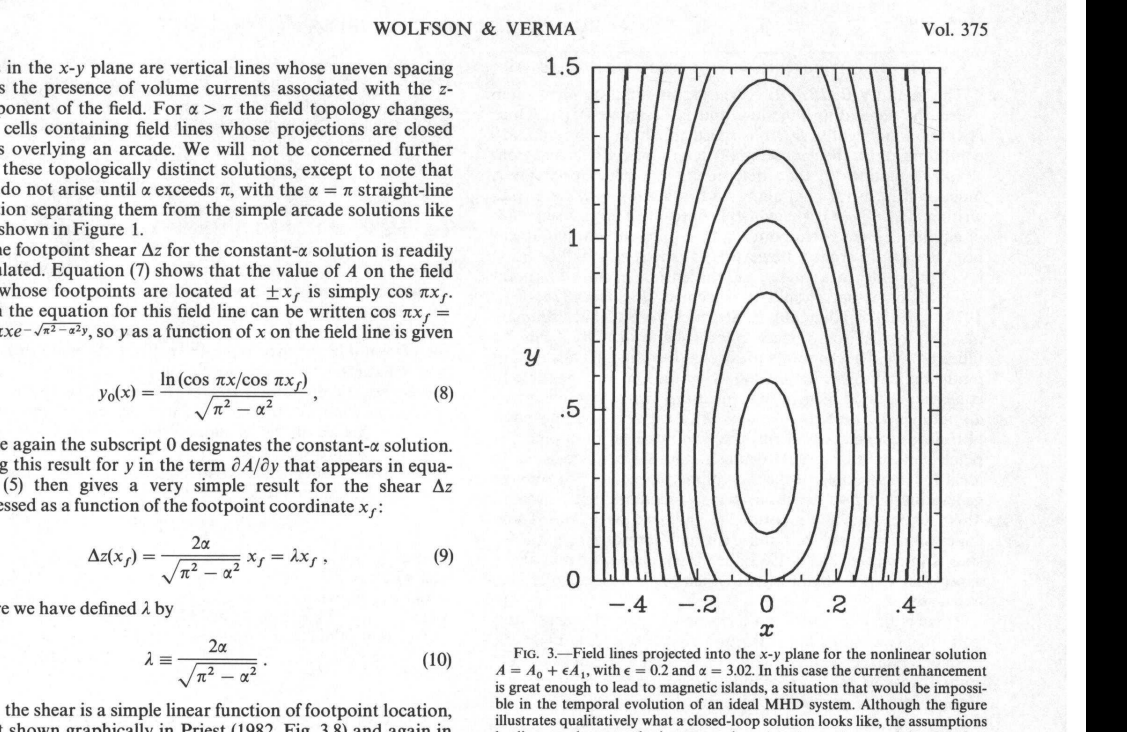
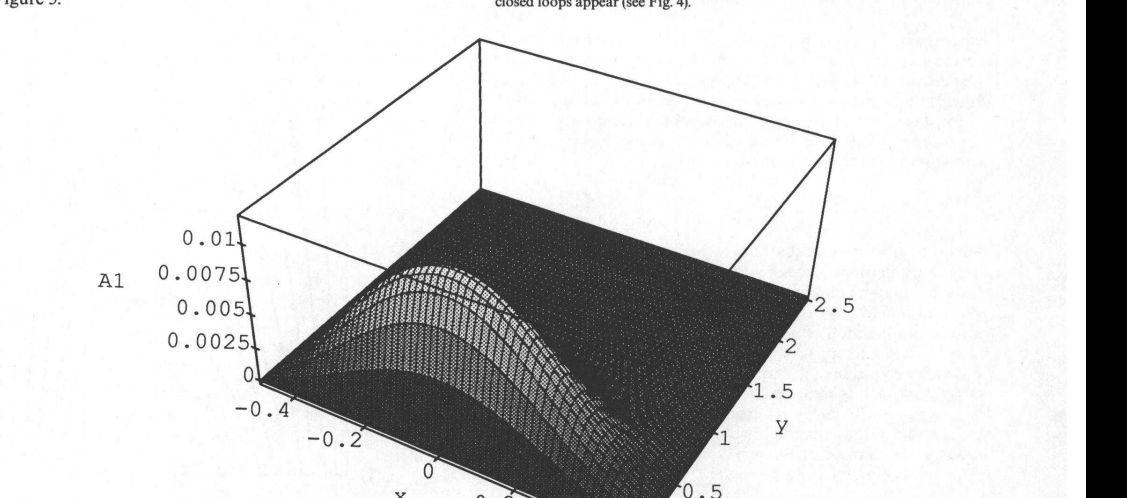
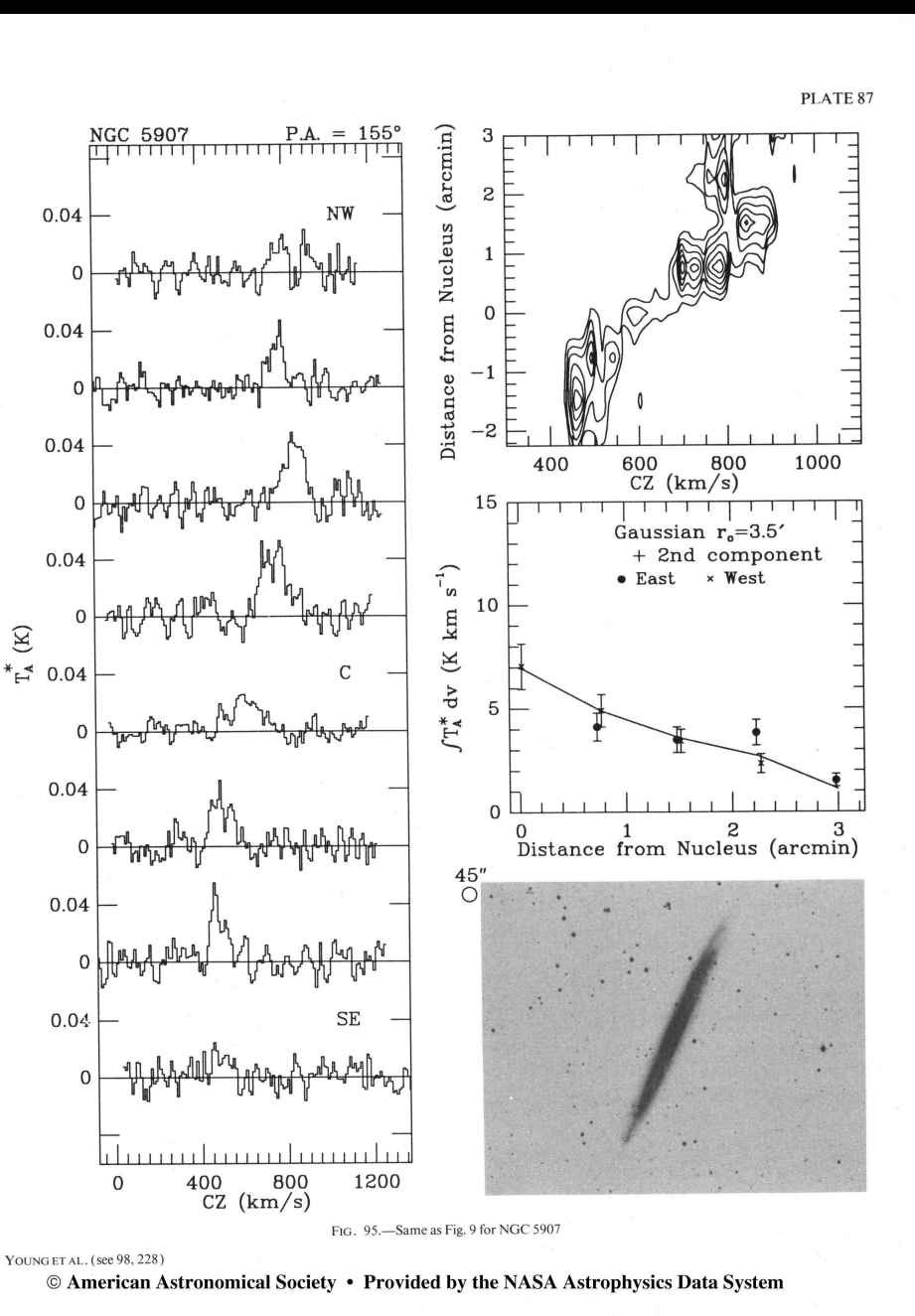


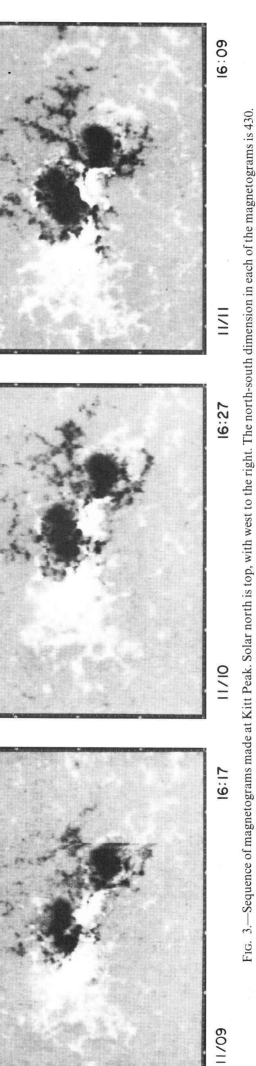
FIG. 3.—Field lines projected into the x-y plane for the nonlinear solution  $A = A_0 + \epsilon A_1$ , with  $\epsilon = 0.2$  and  $x = 3.02$ . In this case the current enhancement is greater than to leave the vessel open, a condition which should be impossible in the temporal evolution of an ideal MHD system. Although this figure illustrates qualitatively what a closed-loop solution looks like, the assumptions leading to the perturbation expansion  $A = A_0 + \epsilon A_1$  are violated before closed loops appear (see Fig. 4).



© American Astronomical Society • Provided by the NASA Astrophysics Data System



YOUNG ET AL. (see 98, 228)  
© American Astronomical Society • Provided by the NASA Astrophysics Data System



ATKIN, JONES, AND ZAHL (see page 878)  
FIG. 3.—Sequence of magnetograms made at Kitt Peak. Solar north is top; west to the right. The north-south dimension in each of the magnetograms is 430.

FIG. 4.—Magnetograms made at Kitt Peak

FIG. 5.—Same as Fig. 9 for NGC 5907

FIG. 6.—Same as Fig. 9 for NGC 5907

FIG. 7.—Same as Fig. 9 for NGC 5907

FIG. 8.—Same as Fig. 9 for NGC 5907

FIG. 9.—Same as Fig. 9 for NGC 5907

FIG. 10.—Same as Fig. 9 for NGC 5907

FIG. 11.—Same as Fig. 9 for NGC 5907

FIG. 12.—Same as Fig. 9 for NGC 5907

FIG. 13.—Same as Fig. 9 for NGC 5907

FIG. 14.—Same as Fig. 9 for NGC 5907

FIG. 15.—Same as Fig. 9 for NGC 5907

FIG. 16.—Same as Fig. 9 for NGC 5907

FIG. 17.—Same as Fig. 9 for NGC 5907

FIG. 18.—Same as Fig. 9 for NGC 5907

FIG. 19.—Same as Fig. 9 for NGC 5907

FIG. 20.—Same as Fig. 9 for NGC 5907

FIG. 21.—Same as Fig. 9 for NGC 5907

FIG. 22.—Same as Fig. 9 for NGC 5907

FIG. 23.—Same as Fig. 9 for NGC 5907

FIG. 24.—Same as Fig. 9 for NGC 5907

FIG. 25.—Same as Fig. 9 for NGC 5907

FIG. 26.—Same as Fig. 9 for NGC 5907

FIG. 27.—Same as Fig. 9 for NGC 5907

FIG. 28.—Same as Fig. 9 for NGC 5907

FIG. 29.—Same as Fig. 9 for NGC 5907

FIG. 30.—Same as Fig. 9 for NGC 5907

FIG. 31.—Same as Fig. 9 for NGC 5907

FIG. 32.—Same as Fig. 9 for NGC 5907

FIG. 33.—Same as Fig. 9 for NGC 5907

FIG. 34.—Same as Fig. 9 for NGC 5907

FIG. 35.—Same as Fig. 9 for NGC 5907

FIG. 36.—Same as Fig. 9 for NGC 5907

FIG. 37.—Same as Fig. 9 for NGC 5907

FIG. 38.—Same as Fig. 9 for NGC 5907

FIG. 39.—Same as Fig. 9 for NGC 5907

FIG. 40.—Same as Fig. 9 for NGC 5907

FIG. 41.—Same as Fig. 9 for NGC 5907

FIG. 42.—Same as Fig. 9 for NGC 5907

FIG. 43.—Same as Fig. 9 for NGC 5907

FIG. 44.—Same as Fig. 9 for NGC 5907

FIG. 45.—Same as Fig. 9 for NGC 5907

FIG. 46.—Same as Fig. 9 for NGC 5907

FIG. 47.—Same as Fig. 9 for NGC 5907

FIG. 48.—Same as Fig. 9 for NGC 5907

FIG. 49.—Same as Fig. 9 for NGC 5907

FIG. 50.—Same as Fig. 9 for NGC 5907

FIG. 51.—Same as Fig. 9 for NGC 5907

FIG. 52.—Same as Fig. 9 for NGC 5907

FIG. 53.—Same as Fig. 9 for NGC 5907

FIG. 54.—Same as Fig. 9 for NGC 5907

FIG. 55.—Same as Fig. 9 for NGC 5907

FIG. 56.—Same as Fig. 9 for NGC 5907

FIG. 57.—Same as Fig. 9 for NGC 5907

FIG. 58.—Same as Fig. 9 for NGC 5907

FIG. 59.—Same as Fig. 9 for NGC 5907

# The Dataset

The Astrophysics Data System (ADS): <https://ui.adsabs.harvard.edu/>

The screenshot shows the ADS search interface with the query 'naiman' entered. The search returned 42 results. The results are listed in a table with columns for citation count, author, year, title, and document links. A sidebar on the left shows filters for Authors, Collections, and Refereed status. A histogram on the right shows the distribution of papers by year and refereed status.

QUICK FIELD: Author First Author Abstract Year Fulltext All Search Terms

naiman

Your search returned 42 results

Author +Naiman, J

AUTHORS

- > Naiman, J 42
- > Hernquist, L 16
- > Springel, V 16
- > Vogelsberger, M 16
- > Marinacci, F 15

COLLECTIONS

- astronomy 41
- physics 3
- general 2

REFERRED

- refereed 31
- non-refereed 11

INSTITUTIONS

KEYWORDS

PUBLICATIONS

BIB GROUPS

Show highlights Show abstracts Hide Sidebars Go To Bottom

1 2020arXiv201011227B 2020/10 cited: 1  
The Catalogue for Astrophysical Turbulence Simulations (CATS)  
Berkhout, B.; Appel, S.; Bialy, S. *and 18 more*

2 2020A&C....3300424A 2020/10  
Clustering-informed cinematic astrophysical data visualization with application to the Moon-forming terrestrial synestia  
Aleo, P. D.; Lock, S. J.; Cox, D. J. *and 5 more*

3 2020ApJ...899L..30G 2020/08 cited: 2  
Winds in Star Clusters Drive Kolmogorov Turbulence  
Gallegos-Garcia, Monica; Berkhout, Blakesley; Rosen, Anna L. *and 2 more*

4 2020ApJ...896...66K 2020/06 cited: 1  
The Effects of Metallicity and Abundance Pattern of the ISM on Supernova Feedback  
Karpov, Platon I.; Martizzi, Davide; Macias, Phillip *and 3 more*

5 2020MNRAS.492.5930L 2020/03 cited: 4  
Redshift evolution of the Fundamental Plane relation in the IllustrisTNG simulation  
Lu, Shengdong; Xu, Dandan; Wang, Yunchong *and 7 more*

Add papers to library

Create email notification

Years Citations Reads

refereed non refereed

14  
12  
10  
8  
6  
4  
2

2004 2005 2006 2007 2008 2009 2010 2011 2012 2013 2014 2015 2016 2017 2018 2019 2020

# The Idea

TABLE 1. Multiple ring nebulae observed.

| WR star <sup>a</sup> | HD Number | Date observed | Filter     | Exposure (secs) | Figure |
|----------------------|-----------|---------------|------------|-----------------|--------|
| WR16                 | HD86161   | 16 May 1994   | H $\alpha$ | 1800            | 2      |
| WR30                 | HD94305   | 15 May 1994   | H $\alpha$ | 900             | 3a     |
| WR30                 | -         | 19 May 1994   | [OIII]     | 2100            | 3b     |
| WR40                 | HD96548   | 18 May 1994   | H $\alpha$ | 1950            | 4a     |
| WR40                 | -         | 19 May 1994   | [OIII]     | 2100            | 4b     |
| WR75                 | HD14749   | 17 May 1994   | H $\alpha$ | 2700            | 1a     |
| WR75                 | -         | 17 May 1994   | [OIII]     | 2700            | 1b     |
| WR85                 | HR6392B   | 16 May 1994   | H $\alpha$ | 900             | 5      |

<sup>a</sup> uses the nomenclature of van der Hucht *et al.* (1981).

ejection events. This uses a similar line of argument to that proposed by Balick *et al.* (1992) for using the extended halos of planetary nebulae to distinguish the characteristics of the red giant stellar winds that existed prior to their formation.

In this paper, we provide new, deep imaging of a number of multiple rings observed around WR stars in an optical narrow-band survey made of WR stars in the southern skies. We discuss their possible implications for WR evolution and postulate what further information they may provide about the evolution of massive stars with closer investigation.

## 2. OBSERVATIONS

Narrow-band imaging, using H $\alpha$  ( $\lambda=6563\text{ \AA}$ ,  $\Delta\lambda=12\text{ \AA}$ ) and [O III] ( $\lambda=5006\text{ \AA}$ ,  $\Delta\lambda=44\text{ \AA}$ ) filters was performed using a Thomson 1024 $\times$ 1024 CCD chip at the f/3 focus of the 0.6 m Curtis Schmidt at Cerro Tololo Interamerican Observatory (CTIO) during the nights of 15–19 May 1994. The sample objects were taken from the lists of Marston *et al.* (1994) and Marston & Yocum (in preparation). It was intended that all possible shells associated with the WR stars would be identified as well as information on relative sizes and morphologies. A full listing of observations used in this paper are supplied in Table 1.

## 3. RESULTS ON MULTIPLE RINGS

Images of the multiple ring systems of our sample are shown in Figs. 1–5. These reveal nebulae whose morphologies allow a classification into two distinct types. Those with bipolar shapes in an outer ejecta shell, and those with more spherical outer shells. Table 2 lists the ring type (after Chu 1991) and apparent sizes of the multiple shells.

### 3.1 Bipolar Shells

Figures 1(a) and 1(b) show new, deep images of the nebula RCW 104 in both H $\alpha$  and [O III] which surrounds the WR star WR75. This is the only object in our sample to show a bipolar morphology in H $\alpha$ . However, close inspection of Fig. 1 of Marston *et al.* (1994) shows that the nebula NGC 2359 around the star WR6 has a diffuse outer, bipolar shell, which extends to approximately 20' from the central star. The bright shell in the center is only 5' across. NGC 2359 has been shown to have multiple velocity components which may be associated with multiple ejections (Goudis *et al.* 1994). Ejected material appears to be interacting with the diffuse bipolar materials as well as a nearby molecular cloud (Marston 1991; Schneps *et al.* 1981). The shell around

WR75 shows similar multiple components. An outer bipolar flow is outlined by strong H $\alpha$  filaments in the central regions while fainter lobes are observed to the north and south, extending to around 15' from the central WN6 star. An inner ring of [O III] emitting material is observed entirely within the bipolar outflow and is only 10' in diameter. The outer filaments of RCW 104 have been spectroscopically observed by Esteban *et al.* (1990), who suggest their abundances are similar to that expected from the enhanced abundances in a RSG wind. We might interpret our observations of these two bipolar nebulae as being the RSG ejecta outer filaments and relatively young WR winds interacting with the ejecta to form central cavities. The expansion of the cavities has not yet reached the edge of the RSG ejecta.

In both cases of bipolar morphology, a wind-blown (W)

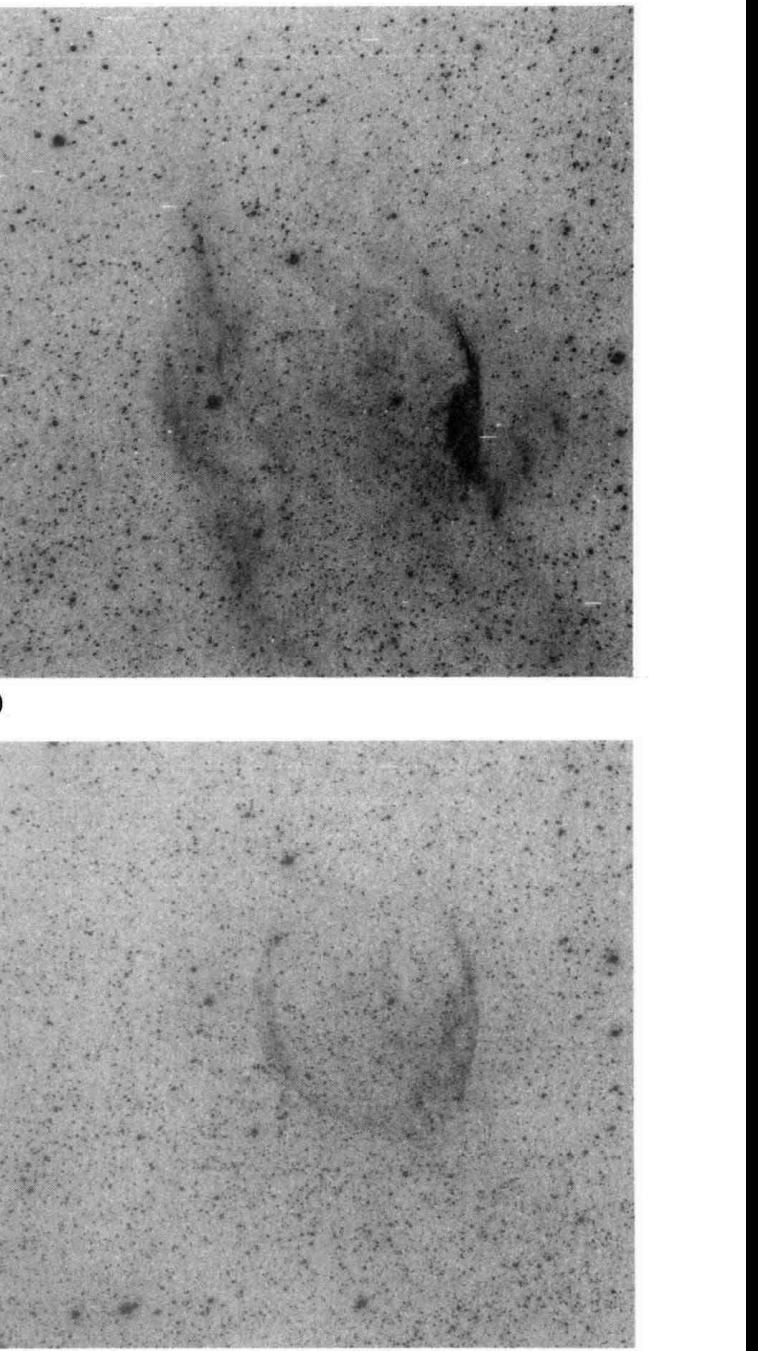


FIG. 1. (a) H $\alpha$  image of the filamentary, bipolar nebula RCW104 surrounding the WR star WR75. (b) Deep [O III] image of the wind-blown bubble at the center of RCW104.

# The Idea

| TABLE 1. Multiple ring nebulae observed. |           |               |            |                 |        |  |
|--|-----------|---------------|------------|-----------------|--------|--|
| WR star <sup>a</sup>                     | HD Number | Date observed | Filter     | Exposure (secs) | Figure |  |
| WR16                                     | HD86161   | 16 May 1994   | H $\alpha$ | 1800            | 2      |  |
| WR30                                     | HD94305   | 15 May 1994   | H $\alpha$ | 900             | 3a     |  |
| WR30                                     | -         | 19 May 1994   | [OIII]     | 2100            | 3b     |  |
| WR40                                     | HD96548   | 18 May 1994   | H $\alpha$ | 1950            | 4a     |  |
| WR40                                     | -         | 19 May 1994   | [OIII]     | 2100            | 4b     |  |
| WR75                                     | HD14749   | 17 May 1994   | H $\alpha$ | 2700            | 1a     |  |
| WR75                                     | -         | 17 May 1994   | [OIII]     | 2700            | 1b     |  |
| WR85                                     | HR6392B   | 16 May 1994   | H $\alpha$ | 900             | 5      |  |

<sup>a</sup> uses the nomenclature of van der Hucht *et al.* (1981).

ejection events. This uses a similar line of argument to that proposed by Balick *et al.* (1992) for using the extended halos of planetary nebulae to distinguish the characteristics of the red giant stellar winds that existed prior to their formation.

In this paper, we provide new, deep imaging of a number of multiple rings observed around WR stars in an optical narrow-band survey made of WR stars in the southern skies. We discuss their possible implications for WR evolution and postulate what further information they may provide about the evolution of massive stars with closer investigation.

## 2. OBSERVATIONS

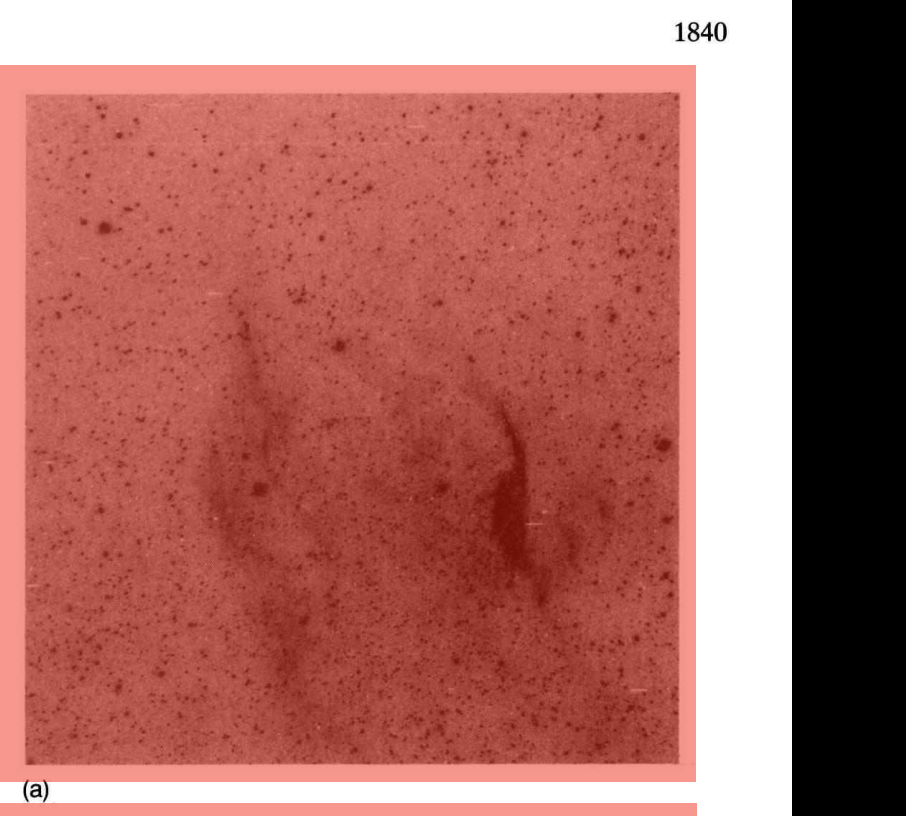
Narrow-band imaging, using H $\alpha$  ( $\lambda=6563\text{ \AA}$ ,  $\Delta\lambda=12\text{ \AA}$ ) and [O III] ( $\lambda=5006\text{ \AA}$ ,  $\Delta\lambda=44\text{ \AA}$ ) filters was performed using a Thomson 1024 $\times$ 1024 CCD chip at the f/3 focus of the 0.6 m Curtis Schmidt at Cerro Tololo Interamerican Observatory (CTIO) during the nights of 15–19 May 1994. The sample objects were taken from the lists of Marston *et al.* (1994) and Marston & Yocum (in preparation). It was intended that all possible shells associated with the WR stars would be identified as well as information on relative sizes and morphologies. A full listing of observations used in this paper are supplied in Table 1.

## 3. RESULTS ON MULTIPLE RINGS

Images of the multiple ring systems of our sample are shown in Figs. 1–5. These reveal nebulae whose morphologies allow a classification into two distinct types. Those with bipolar shapes in an outer ejecta shell, and those with more spherical outer shells. Table 2 lists the ring type (after Chu 1991) and apparent sizes of the multiple shells.

### 3.1 Bipolar Shells

Figures 1(a) and 1(b) show new, deep images of the nebula RCW 104 in both H $\alpha$  and [O III] which surrounds the WR star WR75. This is the only object in our sample to show a bipolar morphology in H $\alpha$ . However, close inspection of Fig. 1 of Marston *et al.* (1994) shows that the nebula NGC 2359 around the star WR6 has a diffuse outer, bipolar shell, which extends to approximately 20' from the central star. The bright shell in the center is only 5' across. NGC 2359 has been shown to have multiple velocity components which may be associated with multiple ejections (Goudis *et al.* 1994). Ejected material appears to be interacting with the diffuse bipolar materials as well as a nearby molecular cloud (Marston 1991; Schneps *et al.* 1981). The shell around



1840

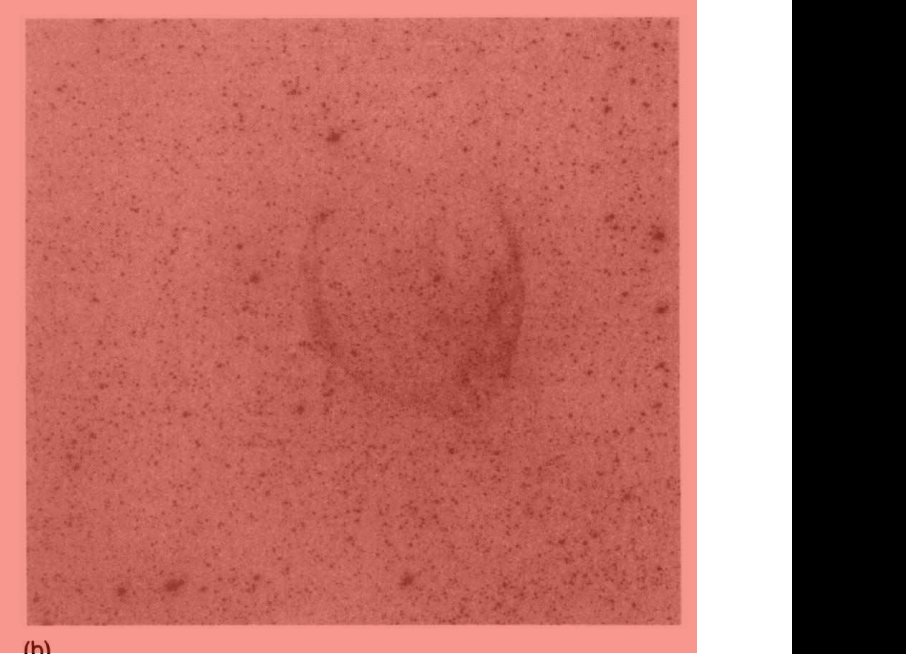


FIG. 1. (a) H $\alpha$  image of the filamentary, bipolar nebula RCW104 surrounding the WR star WR75. (b) Deep [O III] image of the wind-blown bubble at the center of RCW104.

WR75 shows similar multiple components. An outer bipolar flow is outlined by strong H $\alpha$  filaments in the central regions while fainter lobes are observed to the north and south, extending to around 15' from the central WN6 star. An inner ring of [O III] emitting material is observed entirely within the bipolar outflow and is only 10' in diameter. The outer filaments of RCW 104 have been spectroscopically observed by Esteban *et al.* (1990), who suggest their abundances are similar to that expected from the enhanced abundances in a RSG wind. We might interpret our observations of these two bipolar nebulae as being the RSG ejecta outer filaments and relatively young WR winds interacting with the ejecta to form central cavities. The expansion of the cavities has not yet reached the edge of the RSG ejecta.

In both cases of bipolar morphology, a wind-blown (W)

# The Idea

| Table 1. Multiple ring nebulae observed. |         |               |            |                 |        |
|--|---------|---------------|------------|-----------------|--------|
|  | Number  | Date observed | Filter     | Exposure (secs) | Figure |
| WR30                                     | HD94305 | 16 May 1994   | H $\alpha$ | 1800            | 2      |
| WR30                                     | -       | 15 May 1994   | H $\alpha$ | 900             | 3a     |
| WR40                                     | HD96548 | 19 May 1994   | [OIII]     | 2100            | 3b     |
| WR40                                     | -       | 18 May 1994   | H $\alpha$ | 1950            | 4a     |
| WR75                                     | -       | 19 May 1994   | [OIII]     | 2100            | 4b     |
| WR75                                     | HD14749 | 17 May 1994   | H $\alpha$ | 2700            | 1a     |
| WR75                                     | -       | 17 May 1994   | [OIII]     | 2700            | 1b     |
| WR85                                     | HR6392B | 16 May 1994   | H $\alpha$ | 900             | 5      |

<sup>a</sup> uses the nomenclature of van der Hucht *et al.* (1981).

ejection events. This uses a similar line of argument to that proposed by Balick *et al.* (1992) for using the extended halos of planetary nebulae to distinguish the characteristics of the red giant stellar winds that existed prior to their formation.

In this paper, we provide new, deep imaging of a number of multiple rings observed around WR stars in an optical narrow-band survey made of WR stars in the southern skies. We discuss their possible implications for WR evolution and postulate what further information they may provide about the evolution of massive stars with closer investigation.

## 2. OBSERVATIONS

Narrow-band imaging, using H $\alpha$  ( $\lambda=6563 \text{ \AA}$ ,  $\Delta\lambda=12 \text{ \AA}$ ) and [O III] ( $\lambda=5006 \text{ \AA}$ ,  $\Delta\lambda=44 \text{ \AA}$ ) filters was performed using a Thomson 1024 $\times$ 1024 CCD chip at the f/3 focus of the 0.6 m Curtis Schmidt at Cerro Tololo Interamerican Observatory (CTIO) during the nights of 15–19 May 1994. The sample objects were taken from the lists of Marston *et al.* (1994) and Marston & Yocum (in preparation). It was intended that all possible shells associated with the WR stars would be identified as well as information on relative sizes and morphologies. A full listing of observations used in this paper are supplied in Table 1.

## 3. RESULTS ON MULTIPLE RINGS

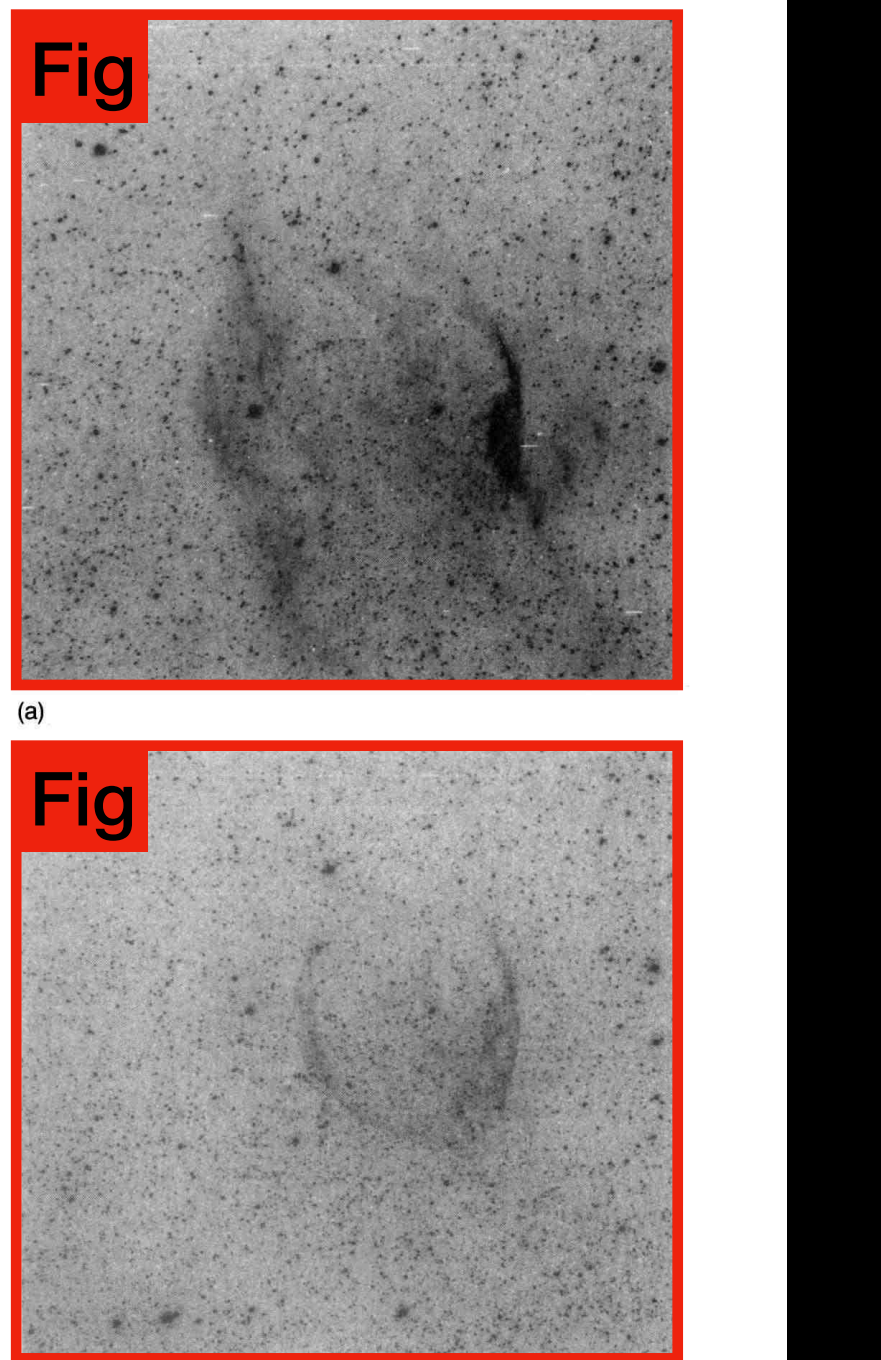
Images of the multiple ring systems of our sample are shown in Figs. 1–5. These figures allow a classification in Fig. 1. (a) H $\alpha$  image of the filamentary, bipolar nebula RCW104 surrounding the WR star WR75. (b) Deep [O III] image of the wind-blown bubble at the center of RCW104.

### Fig Caption

spherical outer shells. Table 2 lists the ring type (after Chu 1991) and apparent sizes of the multiple shells.

#### 3.1 Bipolar Shells

Figures 1(a) and 1(b) show new, deep images of the nebula RCW 104 in both H $\alpha$  and [O III] which surrounds the WR star WR75. This is the only object in our sample to show a bipolar morphology in H $\alpha$ . However, close inspection of Fig. 1 of Marston *et al.* (1994) shows that the nebula NGC 2359 around the star WR6 has a diffuse outer, bipolar shell, which extends to approximately 20' from the central star. The bright shell in the center is only 5' across. NGC 2359 has been shown to have multiple velocity components which may be associated with multiple ejections (Goudis *et al.* 1994). Ejected material appears to be interacting with the diffuse bipolar materials as well as a nearby molecular cloud (Marston 1991; Schneps *et al.* 1981). The shell around



1840

FIG. 1. (a) H $\alpha$  image of the filamentary, bipolar nebula RCW104 surrounding the WR star WR75. (b) Deep [O III] image of the wind-blown bubble at the center of RCW104.

WR75 shows similar multiple components. An outer bipolar flow is outlined by strong H $\alpha$  filaments in the central regions while fainter lobes are observed to the north and south, extending to around 15' from the central WN6 star. An inner ring of [O III] emitting material is observed entirely within the bipolar outflow and is only 10' in diameter. The outer filaments of RCW 104 have been spectroscopically observed by Esteban *et al.* (1990), who suggest their abundances are similar to that expected from the enhanced abundances in a RSG wind. We might interpret our observations of these two bipolar nebulae as being the RSG ejecta outer filaments and relatively young WR winds interacting with the ejecta to form central cavities. The expansion of the cavities has not yet reached the edge of the RSG ejecta.

In both cases of bipolar morphology, a wind-blown (W)

# The Idea

1840 A. R. MARSTON: RINGS AROUND WR STARS

**Table**

Fig 1. Multiple ring nebulae observed.

| Number | Date observed | Filter      | Exposure (secs) | Figure |    |
|--------|---------------|-------------|-----------------|--------|----|
| 61     | 16 May 1994   | H $\alpha$  | 1800            | 2      |    |
| WR30   | HD94305       | 15 May 1994 | H $\alpha$      | 900    | 3a |
| WR30   | -             | 19 May 1994 | [OIII]          | 2100   | 3b |
| WR40   | HD96548       | 18 May 1994 | H $\alpha$      | 1950   | 4a |
| WR40   | -             | 19 May 1994 | [OIII]          | 2100   | 4b |
| WR75   | HD14749       | 17 May 1994 | H $\alpha$      | 2700   | 1a |
| WR75   | -             | 17 May 1994 | [OIII]          | 2700   | 1b |
| WR85   | HR6392B       | 16 May 1994 | H $\alpha$      | 900    | 5  |

<sup>a</sup> uses the nomenclature of van der Hucht et al. (1981).

ejection events. This uses a similar line of argument to that proposed by Balick *et al.* (1992) for using the extended halos of planetary nebulae to distinguish the characteristics of the red giant stellar winds that existed prior to their formation.

In this paper, we provide new, deep imaging of a number of multiple rings observed around WR stars in an optical narrow-band survey made of WR stars in the southern skies. We discuss their possible implications for WR evolution and postulate what further information they may provide about the evolution of massive stars with closer investigation.

2. OBSERVATIONS

Narrow-band imaging, using H $\alpha$  ( $\lambda=6563 \text{ \AA}$ ,  $\Delta\lambda=12 \text{ \AA}$ ) and [O III] ( $\lambda=5006 \text{ \AA}$ ,  $\Delta\lambda=44 \text{ \AA}$ ) filters was performed using a Thomson 1024 $\times$ 1024 CCD chip at the f/3 focus of the 0.6 m Curtis Schmidt at Cerro Tololo Interamerican Observatory (CTIO) during the nights of 15–19 May 1994. The sample objects were taken from the lists of Marston *et al.* (1994) and Marston & Yocum (in preparation). It was intended that all possible shells associated with the WR stars would be identified as well as information on relative sizes and morphologies. A full listing of observations used in this paper are supplied in Table 1.

3. RESULTS ON MULTIPLE RINGS

Images of the multiple ring systems of our sample are shown in Figs. 1–5. These figures allow a classification in Fig Caption bipolar shapes in an outer spherical outer shells. Table 2 lists the ring type (after Chu 1991) and apparent sizes of the multiple shells.

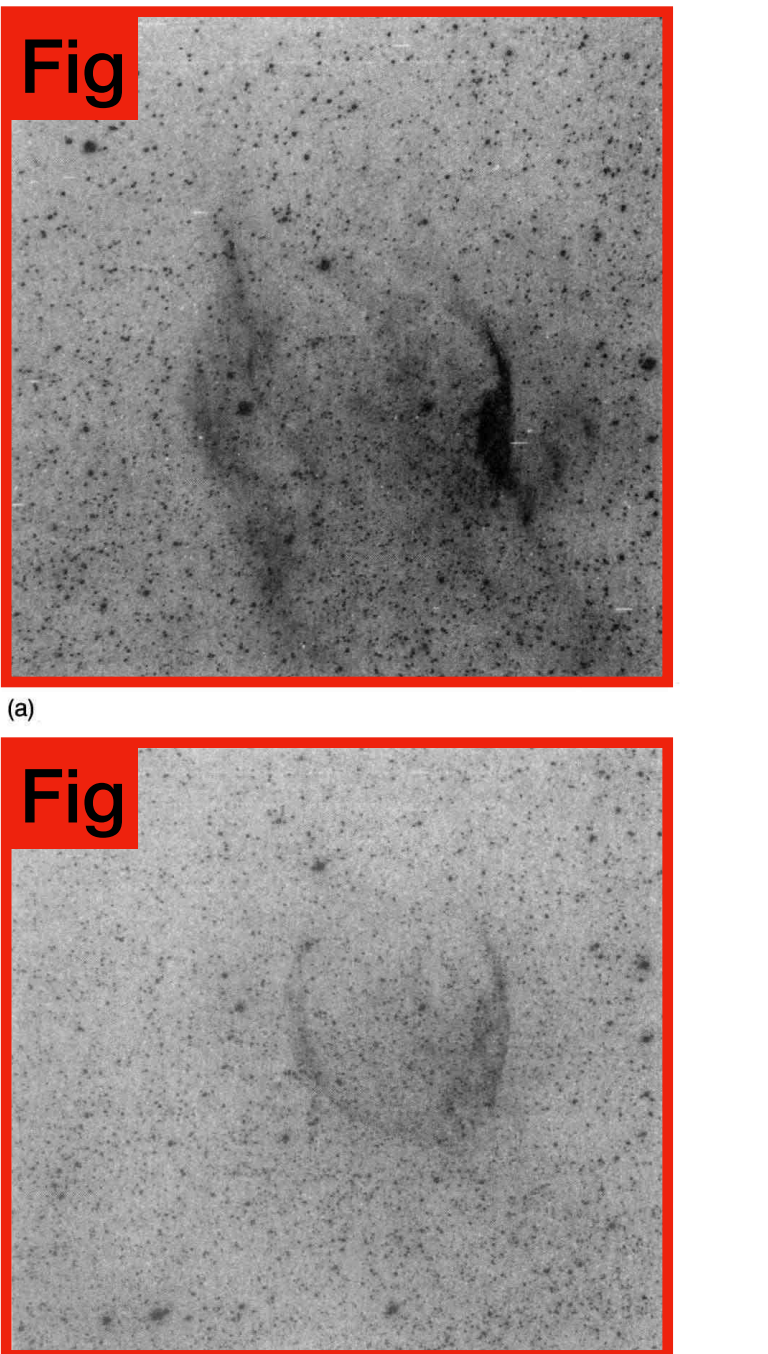
3.1 Bipolar Shells

Figures 1(a) and 1(b) show new, deep images of the nebula RCW 104 in both H $\alpha$  and [O III] which surrounds the WR star WR75. This is the only object in our sample to show a bipolar morphology in H $\alpha$ . However, close inspection of Fig. 1 of Marston *et al.* (1994) shows that the nebula NGC 2359 around the star WR6 has a diffuse outer, bipolar shell, which extends to approximately 20' from the central star. The bright shell in the center is only 5' across. NGC 2359 has been shown to have multiple velocity components which may be associated with multiple ejections (Goudis *et al.* 1994). Ejected material appears to be interacting with the diffuse bipolar materials as well as a nearby molecular cloud (Marston 1991; Schneps *et al.* 1981). The shell around

WR75 shows similar multiple components. An outer bipolar flow is outlined by strong H $\alpha$  filaments in the central regions while fainter lobes are observed to the north and south, extending to around 15' from the central WN6 star. An inner ring of [O III] emitting material is observed entirely within the bipolar outflow and is only 10' in diameter. The outer filaments of RCW 104 have been spectroscopically observed by Esteban *et al.* (1990), who suggest their abundances are similar to that expected from the enhanced abundances in a RSG wind. We might interpret our observations of these two bipolar nebulae as being the RSG ejecta outer filaments and relatively young WR winds interacting with the ejecta to form central cavities. The expansion of the cavities has not yet reached the edge of the RSG ejecta.

In both cases of bipolar morphology, a wind-blown (W)

FIG. 1. (a) H $\alpha$  image of the filamentary, bipolar nebula RCW104 surrounding the WR star WR75. (b) Deep [O III] image of the wind-blown bubble at the center of RCW104.



# The Idea

1840 A. R. MARSTON: RINGS AROUND WR STARS

**Table** Fig. 1. Multiple ring nebulae observed.

| Number | Date observed | Filter      | Exposure (secs) | Figure |    |
|--------|---------------|-------------|-----------------|--------|----|
| 61     | 16 May 1994   | H $\alpha$  | 1800            | 2      |    |
| WR30   | HD94305       | 15 May 1994 | H $\alpha$      | 900    | 3a |
| WR30   | -             | 19 May 1994 | [OIII]          | 2100   | 3b |
| WR40   | HD96548       | 18 May 1994 | H $\alpha$      | 1950   | 4a |
| WR40   | -             | 19 May 1994 | [OIII]          | 2100   | 4b |
| WR75   | HD14749       | 17 May 1994 | H $\alpha$      | 2700   | 1a |
| WR75   | -             | 17 May 1994 | [OIII]          | 2700   | 1b |
| WR85   | HR6392B       | 16 May 1994 | H $\alpha$      | 900    | 5  |

<sup>a</sup> uses the nomenclature of van der Hucht et al. (1981).

ejection events. This uses a similar line of argument to that proposed by Balick *et al.* (1992) for using the extended halos of planetary nebulae to distinguish the characteristics of the red giant stellar winds that existed prior to their formation.

In this paper, we provide new, deep imaging of a number of multiple rings observed around WR stars in an optical narrow-band survey made of WR stars in the southern skies. We discuss their possible implications for WR evolution and postulate what further information they may provide about the evolution of massive stars with closer investigation.

2. OBSERVATIONS

Narrow-band imaging, using H $\alpha$  ( $\lambda=6563 \text{ \AA}$ ,  $\Delta\lambda=12 \text{ \AA}$ ) and [O III] ( $\lambda=5006 \text{ \AA}$ ,  $\Delta\lambda=44 \text{ \AA}$ ) filters was performed using a Thomson 1024 $\times$ 1024 CCD chip at the f/3 focus of the 0.6 m Curtis Schmidt at Cerro Tololo Interamerican Observatory (CTIO) during the nights of 15–19 May 1994. The sample objects were taken from the lists of Marston *et al.* (1994) and Marston & Yocum (in preparation). It was intended that all possible shells associated with the WR stars would be identified as well as information on relative sizes and morphologies. A full listing of observations used in this paper are supplied in Table 1.

3. RESULTS ON MULTIPLE RINGS

Images of the multiple ring systems of our sample are shown in Figs. 1–5. These figures allow a classification in bipolar shapes in an outer spherical outer shells. Table 2 lists the ring type (after Chu 1991) and apparent sizes of the multiple shells.

3.1 Bipolar Shells

Figures 1(a) and 1(b) show new, deep images of the nebula RCW 104 in both H $\alpha$  and [O III] which surrounds the WR star WR75. This is the only object in our sample to show a bipolar morphology in H $\alpha$ . However, close inspection of Fig. 1 of Marston *et al.* (1994) shows that the nebula NGC 2359 around the star WR6 has a diffuse outer, bipolar shell, which extends to approximately 20' from the central star. The bright shell in the center is only 5' across. NGC 2359 has been shown to have multiple velocity components which may be associated with multiple ejections (Goudis *et al.* 1994). Ejected material appears to be interacting with the diffuse bipolar materials as well as a nearby molecular cloud (Marston 1991; Schneps *et al.* 1981). The shell around

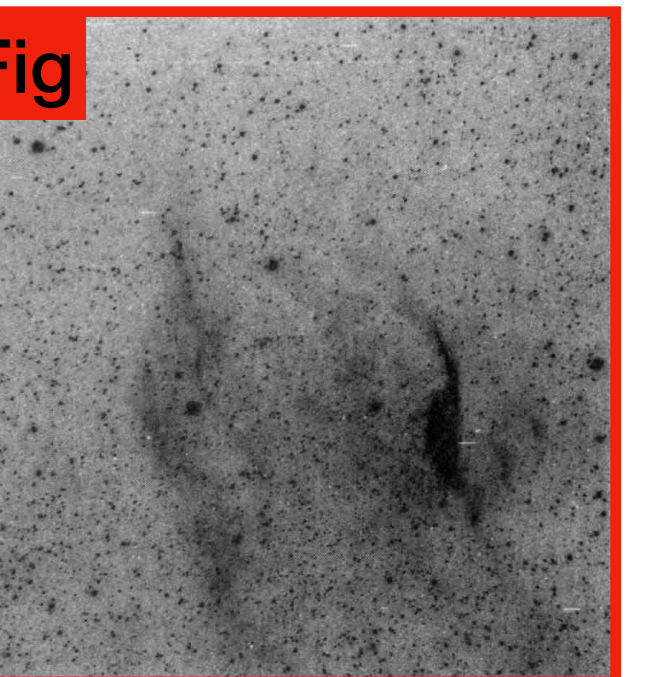
Fig. 1. (a) H $\alpha$  image of the filamentary, bipolar nebula RCW104 surrounding the WR star WR75. (b) Deep [O III] image of the wind-blown bubble at the center of RCW104.

WR75 shows similar multiple components. An outer bipolar flow is outlined by strong H $\alpha$  filaments in the central regions while fainter lobes are observed to the north and south, extending to around 15' from the central WN6 star. An inner ring of [O III] emitting material is observed entirely within the bipolar outflow and is only 10' in diameter. The outer filaments of RCW 104 have been spectroscopically observed by Esteban *et al.* (1990), who suggest their abundances are similar to that expected from the enhanced abundances in a RSG wind. We might interpret our observations of these two bipolar nebulae as being the RSG ejecta outer filaments and relatively young WR winds interacting with the ejecta to form central cavities. The expansion of the cavities has not yet reached the edge of the RSG ejecta.

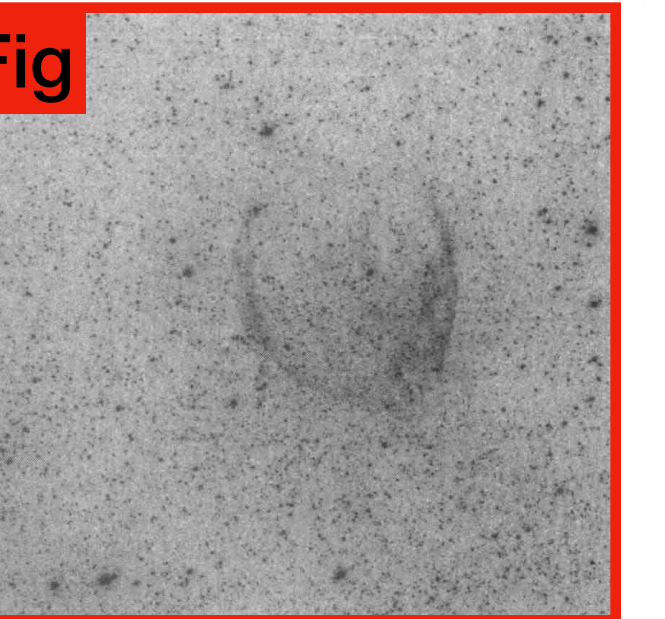
In both cases of bipolar morphology, a wind-blown (W)

CSV File

Get locations of physical objects



(a)



(b)

# The Idea

| Table 1. Multiple ring nebulae observed. |               |            |                 |        |  |
|--|---------------|------------|-----------------|--------|--|
| Number                                   | Date observed | Filter     | Exposure (secs) | Figure |  |
| WR30                                     | 16 May 1994   | H $\alpha$ | 1800            | 2      |  |
| WR30                                     | 15 May 1994   | H $\alpha$ | 900             | 3a     |  |
| WR30                                     | 19 May 1994   | [OIII]     | 2100            | 3b     |  |
| WR40                                     | HD96548       | H $\alpha$ | 1950            | 4a     |  |
| WR40                                     | -             | [OIII]     | 2100            | 4b     |  |
| WR75                                     | HD14749       | H $\alpha$ | 2700            | 1a     |  |
| WR75                                     | -             | [OIII]     | 2700            | 1b     |  |
| WR85                                     | HR6392B       | H $\alpha$ | 900             | 5      |  |

<sup>a</sup> uses the nomenclature of van der Hucht *et al.* (1981).

ejection events. This uses a similar line of argument to that proposed by Balick *et al.* (1992) for using the extended halos of planetary nebulae to distinguish the characteristics of the red giant stellar winds that existed prior to their formation.

In this paper, we provide new, deep imaging of a number of multiple rings observed around WR stars in an optical narrow-band survey made of WR stars in the southern skies. We discuss their possible implications for WR evolution and postulate what further information they may provide about the evolution of massive stars with closer investigation.

## 2. OBSERVATIONS

Narrow-band imaging, using H $\alpha$  ( $\lambda=6563\text{ \AA}$ ,  $\Delta\lambda=12\text{ \AA}$ ) and [O III] ( $\lambda=5006\text{ \AA}$ ,  $\Delta\lambda=44\text{ \AA}$ ) filters was performed using a Thomson 1024 $\times$ 1024 CCD chip at the f/3 focus of the 0.6 m Curtis Schmidt at Cerro Tololo Interamerican Observatory (CTIO) during the nights of 15–19 May 1994. The sample objects were taken from the lists of Marston *et al.* (1994) and Marston & Yocum (in preparation). It was intended that all possible shells associated with the WR stars would be identified as well as information on relative sizes and morphologies. A full listing of observations used in this paper are supplied in Table 1.

## 3. RESULTS ON MULTIPLE RINGS

Images of the multiple ring systems of our sample are shown in Figs. 1–5. These images allow a classification in bipolar shapes in an outer envelope of spherical outer shells. Table 2 lists the ring type (after Chu 1991) and apparent sizes of the multiple shells.

### 3.1 Bipolar Shells

Figures 1(a) and 1(b) show new, deep images of the nebula RCW 104 in both H $\alpha$  and [O III] which surrounds the WR star WR75. This is the only object in our sample to show a bipolar morphology in H $\alpha$ . However, close inspection of Fig. 1 of Marston *et al.* (1994) shows that the nebula NGC 2359 around the star WR6 has a diffuse outer, bipolar shell, which extends to approximately 20' from the central star. The bright shell in the center is only 5' across. NGC 2359 has been shown to have multiple velocity components which may be associated with multiple ejections (Goudis *et al.* 1994). Ejected material appears to be interacting with the diffuse bipolar materials as well as a nearby molecular cloud (Marston 1991; Schneps *et al.* 1981). The shell around

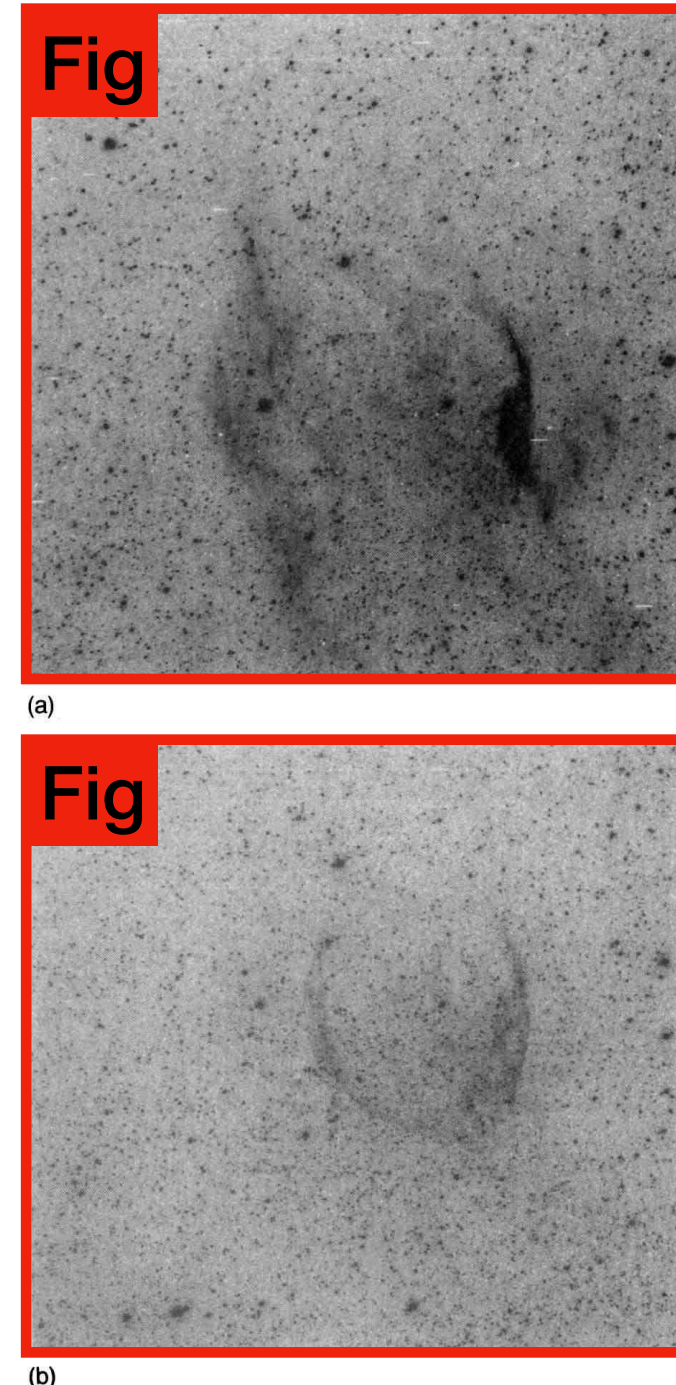
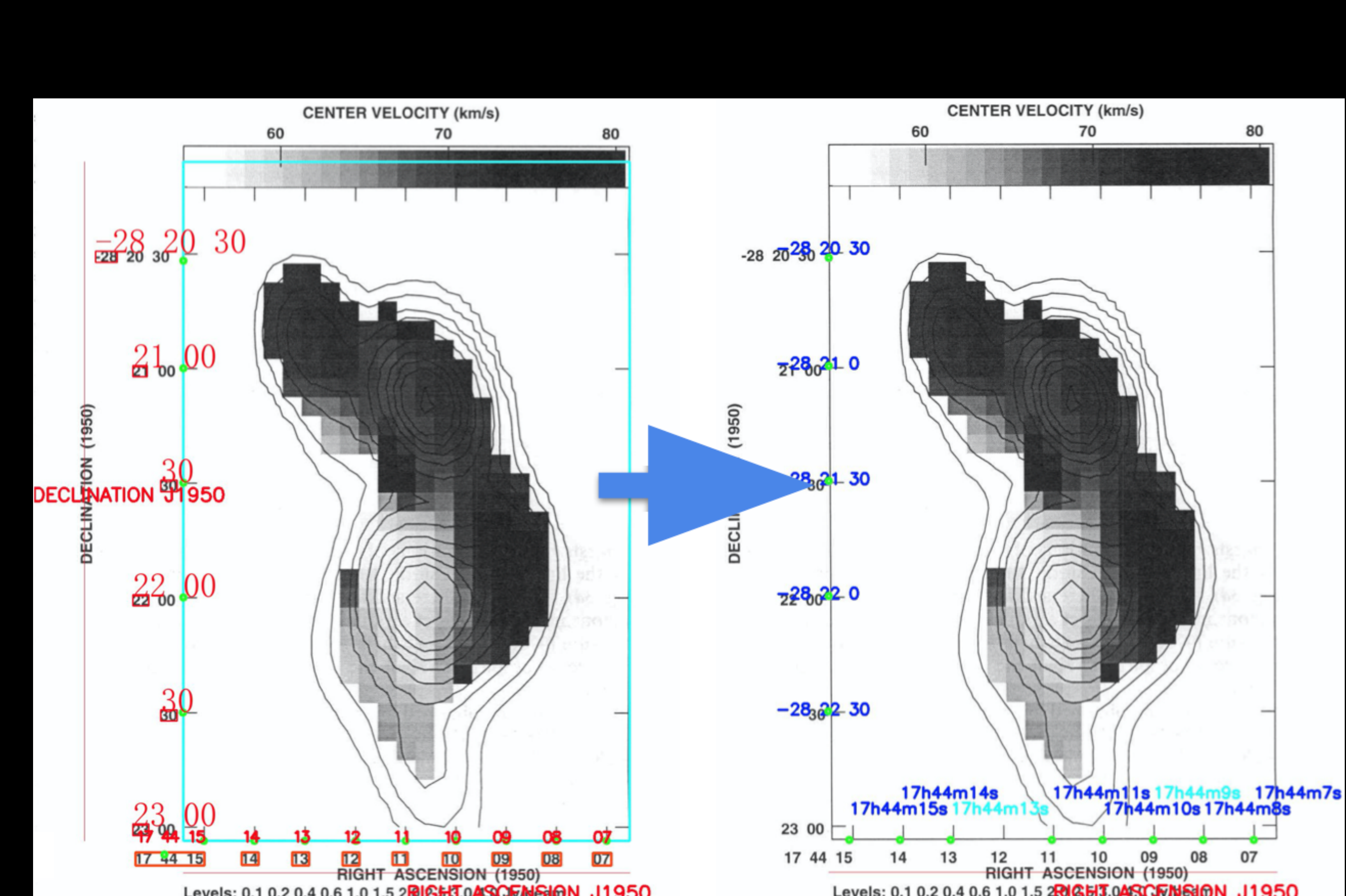


FIG. 1. (a) H $\alpha$  image of the filamentary, bipolar nebula RCW104 surrounding the WR star WR75. (b) Deep [O III] image of the wind-blown bubble at the center of RCW104.

WR75 shows similar multiple components. An outer bipolar flow is outlined by strong H $\alpha$  filaments in the central regions while fainter lobes are observed to the north and south, extending to around 15' from the central WN6 star. An inner ring of [O III] emitting material is observed entirely within the bipolar outflow and is only 10' in diameter. The outer filaments of RCW 104 have been spectroscopically observed by Esteban *et al.* (1990), who suggest their abundances are similar to that expected from the enhanced abundances in a RSG wind. We might interpret our observations of these two bipolar nebulae as being the RSG ejecta outer filaments and relatively young WR winds interacting with the ejecta to form central cavities. The expansion of the cavities has not yet reached the edge of the RSG ejecta.

In both cases of bipolar morphology, a wind-blown (W)



# The Idea : How do we do this?

| Table 1. Multiple ring nebulae observed. |               |            |                 |        |  |
|--|---------------|------------|-----------------|--------|--|
| Number                                   | Date observed | Filter     | Exposure (secs) | Figure |  |
| WR30                                     | 16 May 1994   | H $\alpha$ | 1800            | 2      |  |
| WR30                                     | 15 May 1994   | H $\alpha$ | 900             | 3a     |  |
| WR30                                     | -             | [OIII]     | 2100            | 3b     |  |
| WR40                                     | 18 May 1994   | H $\alpha$ | 1950            | 4a     |  |
| WR40                                     | -             | [OIII]     | 2100            | 4b     |  |
| WR75                                     | 17 May 1994   | H $\alpha$ | 2700            | 1a     |  |
| WR75                                     | -             | [OIII]     | 2700            | 1b     |  |
| WR85                                     | 16 May 1994   | H $\alpha$ | 900             | 5      |  |

<sup>a</sup> uses the nomenclature of van der Hucht et al. (1981).

ejection events. This uses a similar line of argument to that proposed by Balick *et al.* (1992) for using the extended halos of planetary nebulae to distinguish the characteristics of the red giant stellar winds that existed prior to their formation.

In this paper, we provide new, deep imaging of a number of multiple rings observed around WR stars in an optical narrow-band survey made of WR stars in the southern skies. We discuss their possible implications for WR evolution and postulate what further information they may provide about the evolution of massive stars with closer investigation.

## 2. OBSERVATIONS

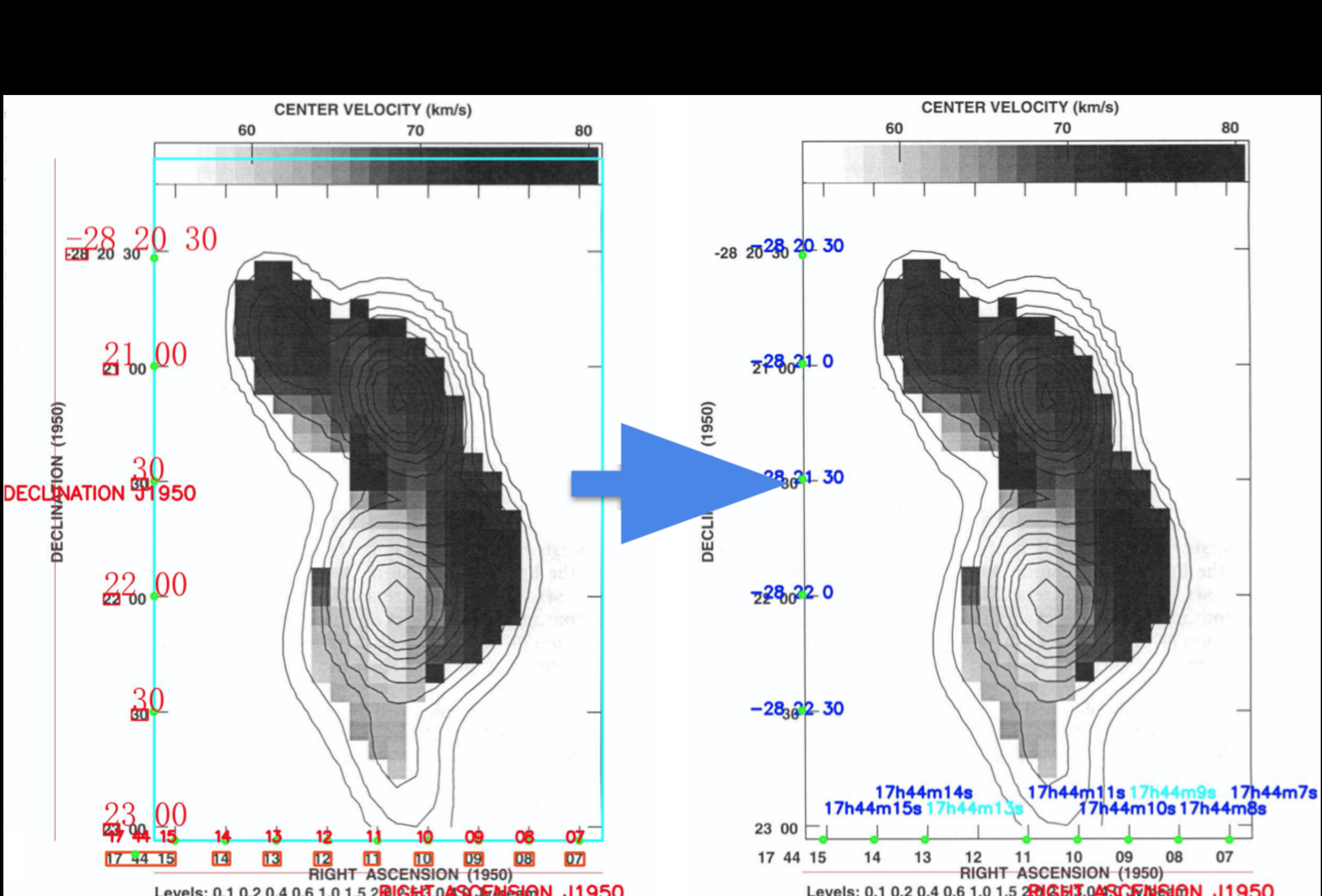
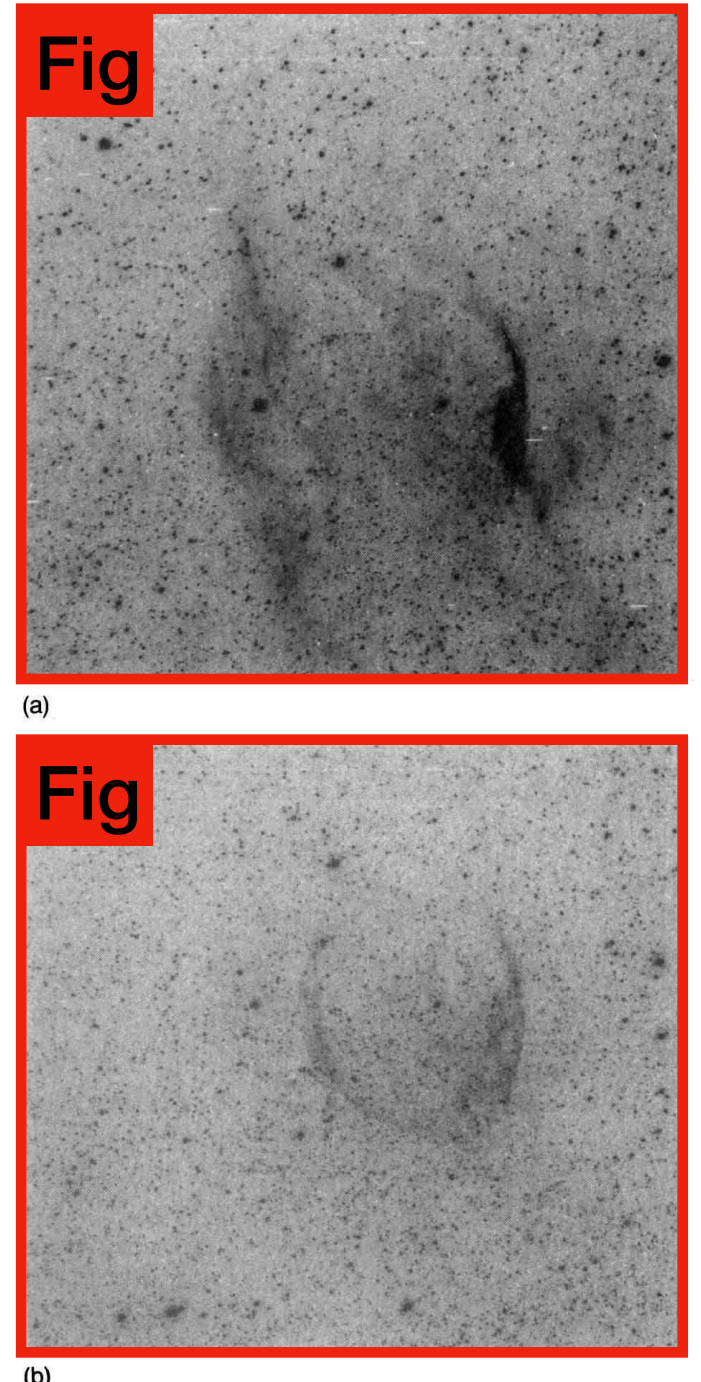
Narrow-band imaging, using H $\alpha$  ( $\lambda=6563 \text{ \AA}$ ,  $\Delta\lambda=12 \text{ \AA}$ ) and [O III] ( $\lambda=5006 \text{ \AA}$ ,  $\Delta\lambda=44 \text{ \AA}$ ) filters was performed using a Thomson 1024 $\times$ 1024 CCD chip at the f/3 focus of the 0.6 m Curtis Schmidt at Cerro Tololo Interamerican Observatory (CTIO) during the nights of 15–19 May 1994. The sample objects were taken from the lists of Marston *et al.* (1994) and Marston & Yocum (in preparation). It was intended that all possible shells associated with the WR stars would be identified as well as information on relative sizes and morphologies. A full listing of observations used in this paper are supplied in Table 1.

## 3. RESULTS ON MULTIPLE RINGS

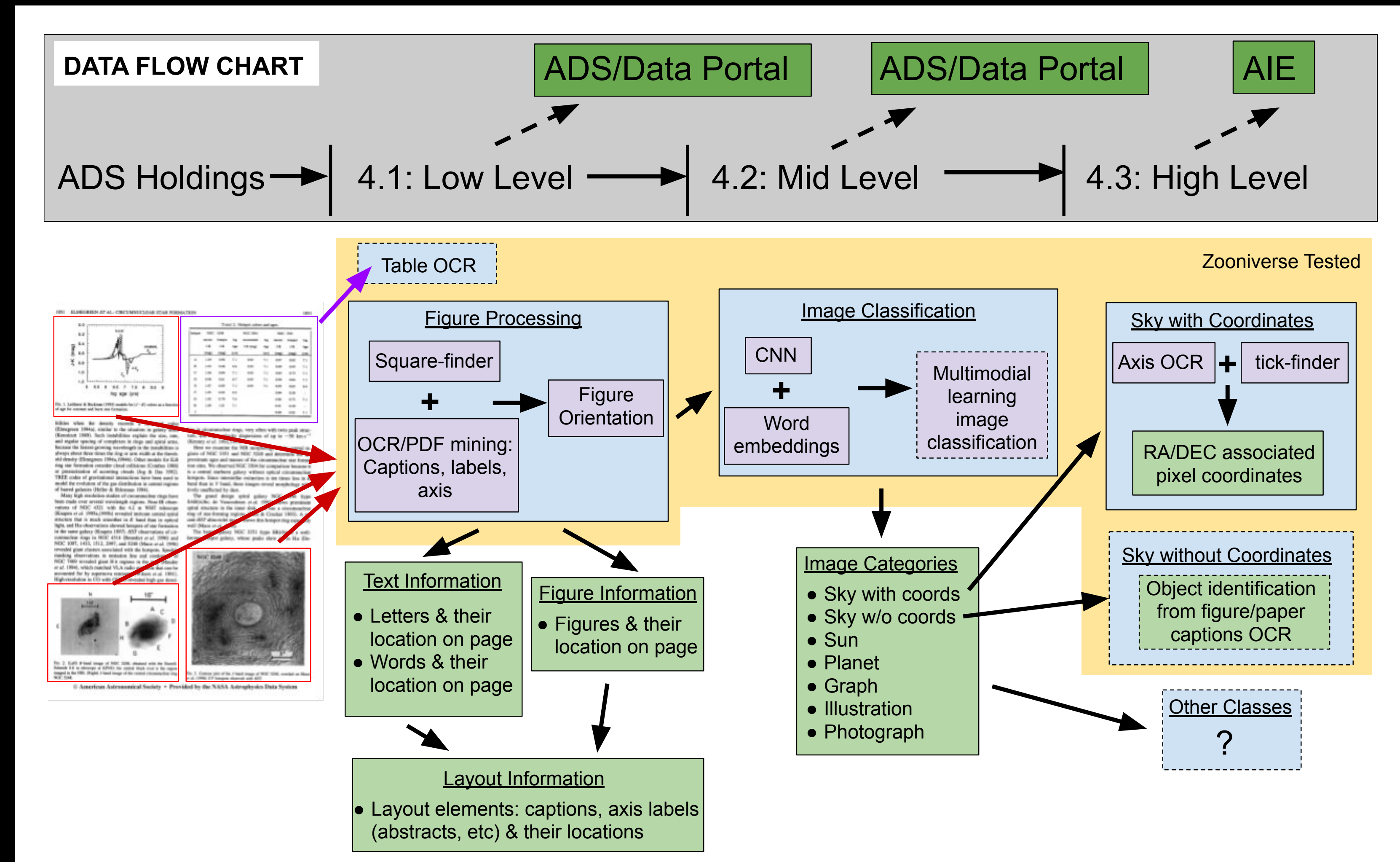
Images of the multiple ring systems of our sample are shown in Figs. 1–5. These images allow a classification in Fig. 6. The morphologies allow a classification in Fig. 7. The spherical outer shells. Table 2 lists the ring type (after Chu 1991) and apparent sizes of the multiple shells.

### 3.1 Bipolar Shells

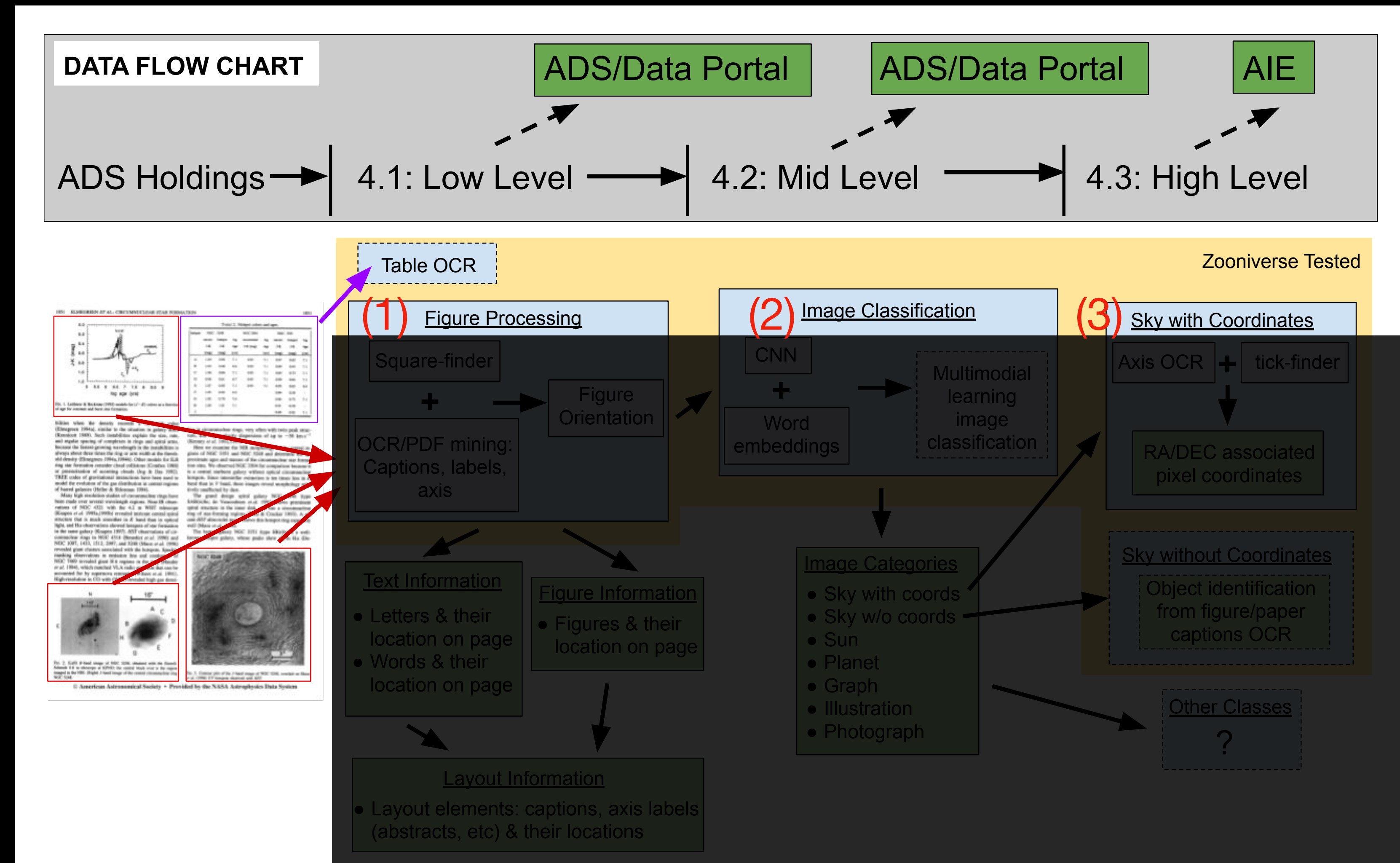
Figures 1(a) and 1(b) show new, deep images of the nebula RCW 104 in both H $\alpha$  and [O III] which surrounds the WR star WR75. This is the only object in our sample to show a bipolar morphology in H $\alpha$ . However, close inspection of Fig. 1 of Marston *et al.* (1994) shows that the nebula NGC 2359 around the star WR6 has a diffuse outer, bipolar shell, which extends to approximately 20' from the central star. The bright shell in the center is only 5' across. NGC 2359 has been shown to have multiple velocity components which may be associated with multiple ejections (Goudis *et al.* 1994). Ejected material appears to be interacting with the diffuse bipolar materials as well as a nearby molecular cloud (Marston 1991; Schneps *et al.* 1981). The shell around



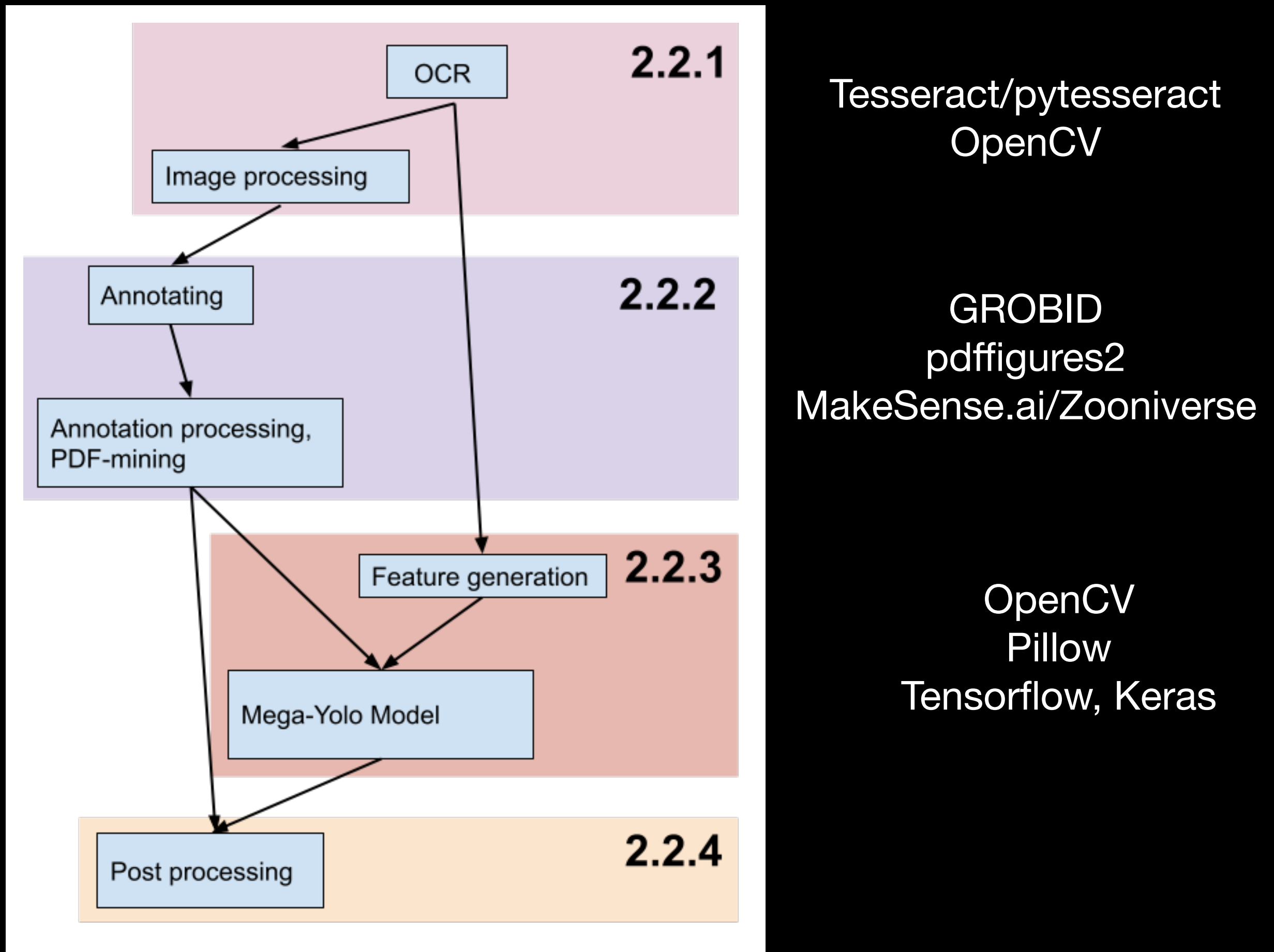
# The Idea : How do we do this?



# The Idea : How do we do this?



# Results of our method



Tesseract/pytesseract  
OpenCV

GROBID  
pdffigures2  
MakeSense.ai/Zooniverse

OpenCV  
Pillow  
Tensorflow, Keras

Naiman et al. (any day now)

# Results of our method

|      | ScanBank<br>No PP |      | ScanBank<br>w/PP |      | detectron2* |                  | detectron2* |                  | Ours<br>No PP |      | Ours<br>w/PP |      |
|------|-------------------|------|------------------|------|-------------|------------------|-------------|------------------|---------------|------|--------------|------|
|      | fig               | cap  | fig              | cap  | fig         | cap <sup>†</sup> | fig         | cap <sup>†</sup> | fig           | cap  | fig          | cap  |
| TP   | 69.9              | 29.0 | 69.3             | 52.8 | 72.0        | 46.4             | 81.0        | 80.9             | 58.2          | 23.2 | 85.7         | 86.7 |
| FP   | 71.4              | 28.8 | 43.6             | 8.7  | 41.8        | 68.2             | 27.1        | 22.4             | 45.3          | 82.3 | 13.7         | 8.6  |
| FN   | 1.7               | 42.8 | 2.5              | 40.7 | 0.6         | 1.6              | 1.2         | 4.9              | 3.1           | 5.1  | 3.5          | 6.0  |
| Prec | 49.5              | 50.2 | 61.4             | 85.9 | 63.3        | 40.5             | 74.9        | 78.3             | 56.2          | 22.0 | 86.2         | 90.9 |
| Rec  | 97.6              | 40.4 | 96.5             | 56.5 | 99.2        | 96.6             | 98.5        | 94.3             | 95.0          | 81.9 | 96.1         | 93.6 |
| F1   | 65.7              | 44.8 | 75.0             | 68.1 | 77.2        | 57.1             | 85.1        | 85.6             | 70.6          | 34.7 | 90.9         | 92.2 |

Naiman et al. (any day now)

# Results of our method

fig = figure

cap = figure caption

|      | ScanBank |      | ScanBank |      | detectron2* |                  | detectron2* |                  | Ours  |      | Ours |      |
|------|----------|------|----------|------|-------------|------------------|-------------|------------------|-------|------|------|------|
|      | No PP    |      | w/PP     |      | No PP       |                  | w/PP        |                  | No PP |      | w/PP |      |
|      | fig      | cap  | fig      | cap  | fig         | cap <sup>†</sup> | fig         | cap <sup>†</sup> | fig   | cap  | fig  | cap  |
| TP   | 69.9     | 29.0 | 69.3     | 52.8 | 72.0        | 46.4             | 81.0        | 80.9             | 58.2  | 23.2 | 85.7 | 86.7 |
| FP   | 71.4     | 28.8 | 43.6     | 8.7  | 41.8        | 68.2             | 27.1        | 22.4             | 45.3  | 82.3 | 13.7 | 8.6  |
| FN   | 1.7      | 42.8 | 2.5      | 40.7 | 0.6         | 1.6              | 1.2         | 4.9              | 3.1   | 5.1  | 3.5  | 6.0  |
| Prec | 49.5     | 50.2 | 61.4     | 85.9 | 63.3        | 40.5             | 74.9        | 78.3             | 56.2  | 22.0 | 86.2 | 90.9 |
| Rec  | 97.6     | 40.4 | 96.5     | 56.5 | 99.2        | 96.6             | 98.5        | 94.3             | 95.0  | 81.9 | 96.1 | 93.6 |
| F1   | 65.7     | 44.8 | 75.0     | 68.1 | 77.2        | 57.1             | 85.1        | 85.6             | 70.6  | 34.7 | 90.9 | 92.2 |

Naiman et al. (any day now)

# Results of our method

fig = figure

cap = figure caption

|                | ScanBank |      | ScanBank |      | detectron2* |                  | detectron2* |                  | Ours  |      | Ours |      |      |
|----------------|----------|------|----------|------|-------------|------------------|-------------|------------------|-------|------|------|------|------|
|                | No PP    |      | w/PP     |      | No PP       |                  | w/PP        |                  | No PP |      | w/PP |      |      |
|                | fig      | cap  | fig      | cap  | fig         | cap <sup>†</sup> | fig         | cap <sup>†</sup> | fig   | cap  | fig  | cap  |      |
| True Positive  | TP       | 69.9 | 29.0     | 69.3 | 52.8        | 72.0             | 46.4        | 81.0             | 80.9  | 58.2 | 23.2 | 85.7 | 86.7 |
| False Positive | FP       | 71.4 | 28.8     | 43.6 | 8.7         | 41.8             | 68.2        | 27.1             | 22.4  | 45.3 | 82.3 | 13.7 | 8.6  |
| False Negative | FN       | 1.7  | 42.8     | 2.5  | 40.7        | 0.6              | 1.6         | 1.2              | 4.9   | 3.1  | 5.1  | 3.5  | 6.0  |
| Precision      | Prec     | 49.5 | 50.2     | 61.4 | 85.9        | 63.3             | 40.5        | 74.9             | 78.3  | 56.2 | 22.0 | 86.2 | 90.9 |
| Recall         | Rec      | 97.6 | 40.4     | 96.5 | 56.5        | 99.2             | 96.6        | 98.5             | 94.3  | 95.0 | 81.9 | 96.1 | 93.6 |
|                | F1       | 65.7 | 44.8     | 75.0 | 68.1        | 77.2             | 57.1        | 85.1             | 85.6  | 70.6 | 34.7 | 90.9 | 92.2 |

Naiman et al. (any day now)

# Results of our method

fig = figure

cap = figure caption

|                | ScanBank |      | ScanBank |      | detectron2* |                  | detectron2* |                  | Ours  |      | Ours |      |      |
|----------------|----------|------|----------|------|-------------|------------------|-------------|------------------|-------|------|------|------|------|
|                | No PP    |      | w/PP     |      | No PP       |                  | w/PP        |                  | No PP |      | w/PP |      |      |
|                | fig      | cap  | fig      | cap  | fig         | cap <sup>†</sup> | fig         | cap <sup>†</sup> | fig   | cap  | fig  | cap  |      |
| True Positive  | TP       | 69.9 | 29.0     | 69.3 | 52.8        | 72.0             | 46.4        | 81.0             | 80.9  | 58.2 | 23.2 | 85.7 | 86.7 |
| False Positive | FP       | 71.4 | 28.8     | 43.6 | 8.7         | 41.8             | 68.2        | 27.1             | 22.4  | 45.3 | 82.3 | 13.7 | 8.6  |
| False Negative | FN       | 1.7  | 42.8     | 2.5  | 40.7        | 0.6              | 1.6         | 1.2              | 4.9   | 3.1  | 5.1  | 3.5  | 6.0  |
| Precision      | Prec     | 49.5 | 50.2     | 61.4 | 85.9        | 63.3             | 40.5        | 74.9             | 78.3  | 56.2 | 22.0 | 86.2 | 90.9 |
| Recall         | Rec      | 97.6 | 40.4     | 96.5 | 56.5        | 99.2             | 96.6        | 98.5             | 94.3  | 95.0 | 81.9 | 96.1 | 93.6 |
|                | F1       | 65.7 | 44.8     | 75.0 | 68.1        | 77.2             | 57.1        | 85.1             | 85.6  | 70.6 | 34.7 | 90.9 | 92.2 |

Naiman et al. (any day now)

# Results of our method

fig = figure

cap = figure caption

|                | ScanBank |      | ScanBank |      | detectron2* |                  | detectron2* |                  | Ours  |      | Ours  |      |      |
|----------------|----------|------|----------|------|-------------|------------------|-------------|------------------|-------|------|-------|------|------|
|                | No PP    | w/PP | No PP    | w/PP | No PP       | w/PP             | No PP       | w/PP             | No PP | w/PP | No PP | w/PP |      |
|                | fig      | cap  | fig      | cap  | fig         | cap <sup>†</sup> | fig         | cap <sup>†</sup> | fig   | cap  | fig   | cap  |      |
| True Positive  | TP       | 69.9 | 29.0     | 69.3 | 52.8        | 72.0             | 46.4        | 81.0             | 80.9  | 58.2 | 23.2  | 85.7 | 86.7 |
| False Positive | FP       | 71.4 | 28.8     | 43.6 | 8.7         | 41.8             | 68.2        | 27.1             | 22.4  | 45.3 | 82.3  | 13.7 | 8.6  |
| False Negative | FN       | 1.7  | 42.8     | 2.5  | 40.7        | 0.6              | 1.6         | 1.2              | 4.9   | 3.1  | 5.1   | 3.5  | 6.0  |
| Precision      | Prec     | 49.5 | 50.2     | 61.4 | 85.9        | 63.3             | 40.5        | 74.9             | 78.3  | 56.2 | 22.0  | 86.2 | 90.9 |
| Recall         | Rec      | 97.6 | 40.4     | 96.5 | 56.5        | 99.2             | 96.6        | 98.5             | 94.3  | 95.0 | 81.9  | 96.1 | 93.6 |
|                | F1       | 65.7 | 44.8     | 75.0 | 68.1        | 77.2             | 57.1        | 85.1             | 85.6  | 70.6 | 34.7  | 90.9 | 92.2 |

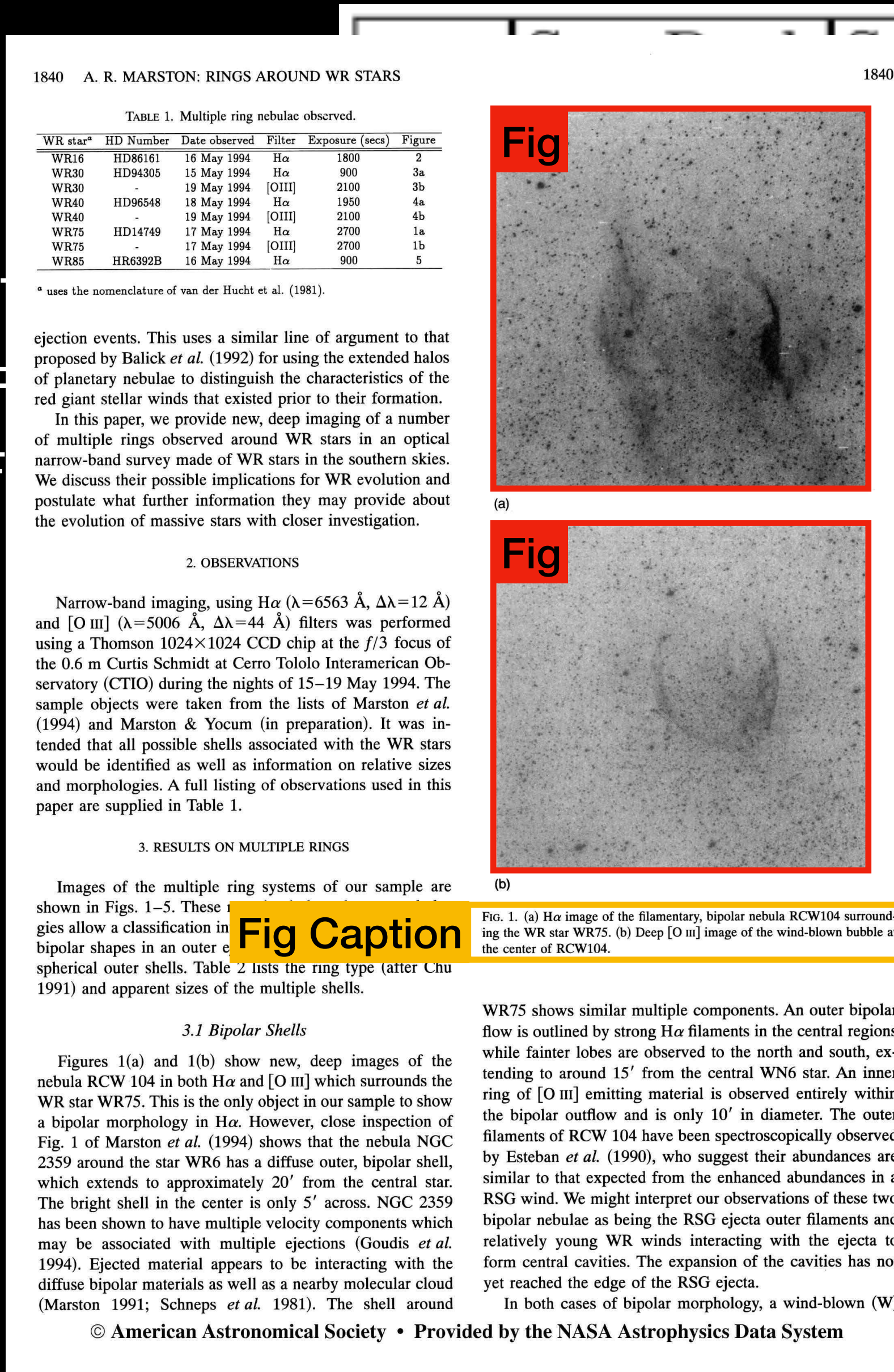
Naiman et al. (any day now)



# Results of our method

fig = figure

cap = figure caption

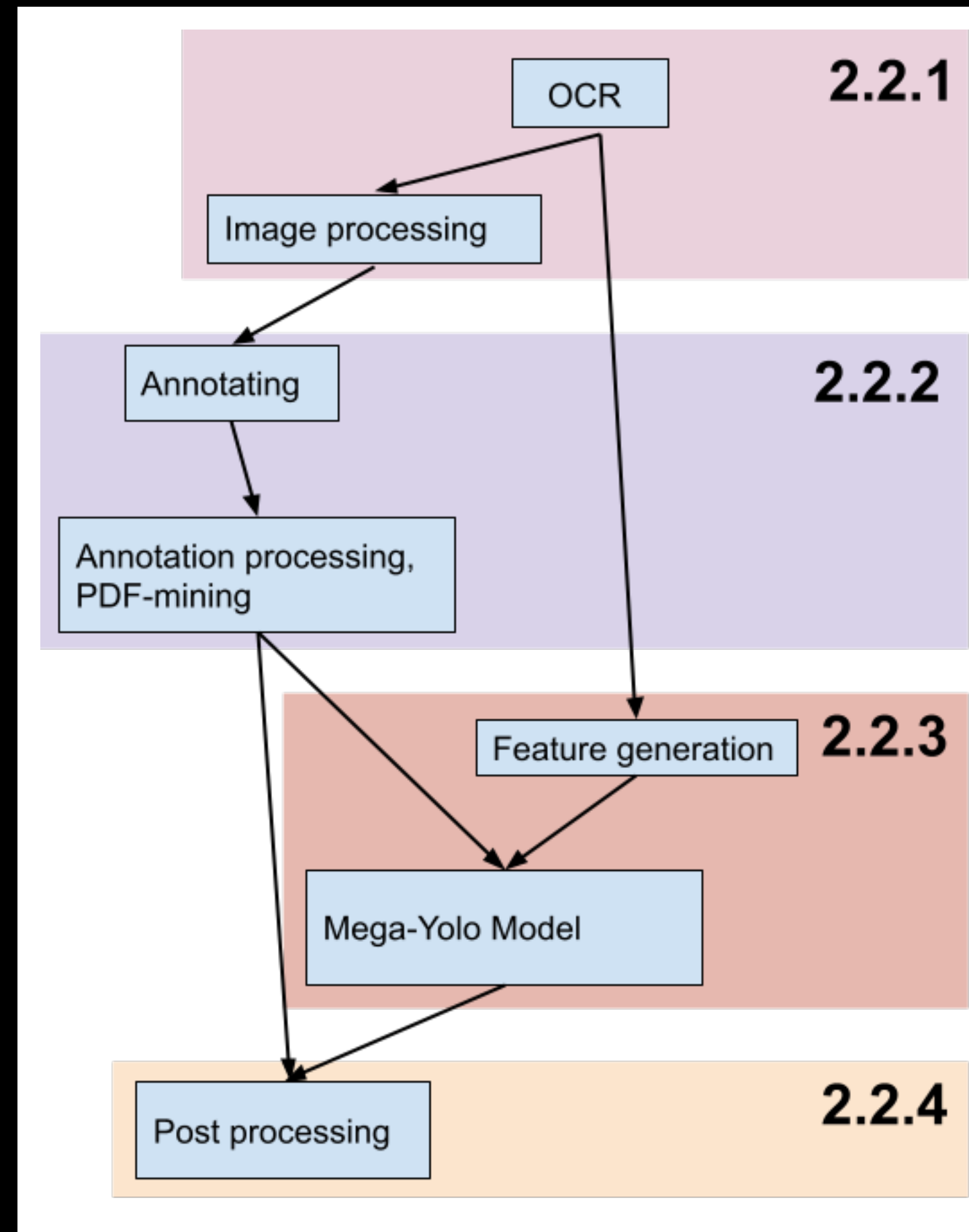


| unBank        |                               | detectron2*                  |                  | detectron2*                  |                 | Ours            |      | Ours |      |
|---------------|-------------------------------|------------------------------|------------------|------------------------------|-----------------|-----------------|------|------|------|
| v/PP<br>; cap | No PP<br>fig cap <sup>†</sup> | w/PP<br>fig cap <sup>†</sup> | No PP<br>fig cap | w/PP<br>fig cap <sup>†</sup> | Ours<br>fig cap | Ours<br>fig cap |      |      |      |
| 3             | 52.8                          | 72.0                         | 46.4             | 81.0                         | 80.9            | 58.2            | 23.2 | 85.7 | 86.7 |
| 6             | 8.7                           | 41.8                         | 68.2             | 27.1                         | 22.4            | 45.3            | 82.3 | 13.7 | 8.6  |
| 5             | 40.7                          | 0.6                          | 1.6              | 1.2                          | 4.9             | 3.1             | 5.1  | 3.5  | 6.0  |
| 4             | 85.9                          | 63.3                         | 40.5             | 74.9                         | 78.3            | 56.2            | 22.0 | 86.2 | 90.9 |
| 5             | 56.5                          | 99.2                         | 96.6             | 98.5                         | 94.3            | 95.0            | 81.9 | 96.1 | 93.6 |
| 0             | 68.1                          | 77.2                         | 57.1             | 85.1                         | 85.6            | 70.6            | 34.7 | 90.9 | 92.2 |

Naiman et al. (any day now)

$$\text{IoU} = \frac{\text{Area of Overlap}}{\text{Area of Union}} = 0.9$$

# Results of our method



Tesseract/pytesseract  
OpenCV



Campus cluster for large batch

GROBID  
pdffigures2  
MakeSense.ai/Zooniverse



Zooniverse scaled for citizen  
scientists  
(Automatically tag machine learning  
method vs citizen science)

OpenCV  
Pillow  
Tensorflow, Keras



AWS

Naiman et al. (any day now)

# Summary & Useful links

[astronaiman.com](http://astronaiman.com)

## Astrophysics

- <https://www.astronaiman.com/publications.html>
- <https://www.tng-project.org/>

## Data Viz

- <https://www.astronaiman.com/vizualization.html>
- <https://www.astroblend.com/> (Blender+Astro Data, hasn't been updated in a while)
- [ytini.com](https://ytini.com)
- <https://yt-project.org/> (scientific data analysis)
- <https://www.sidefx.com/> (Houdini)
- <https://avl.ncsa.illinois.edu/> (Advanced Visualization Lab, NCSA)
- [https://uiuc-ischool-dataviz.github.io/is445\\_spring2022/](https://uiuc-ischool-dataviz.github.io/is445_spring2022/) (this semester's Data Viz course)
- Other courses:
  - <https://www.astroblend.com/ba2016/> & <https://www.astroblend.com/ba2017/>
  - [https://jnaiman.github.io/csci-p-14110\\_su2020/](https://jnaiman.github.io/csci-p-14110_su2020/)
  - [https://jnaiman.github.io/csci-p-14110\\_su2019/](https://jnaiman.github.io/csci-p-14110_su2019/)

## Digitization

- <https://www.astronaiman.com/digitization.html>
- <https://github.com/ReadingTimeMachine> (public with paper publishing)
- Review of document layout analysis: <https://www.mdpi.com/2076-3417/11/12/5344>















